ELSEVIER

Contents lists available at ScienceDirect

### **Chemical Geology**

journal homepage: www.elsevier.com/locate/chemgeo





# Enriched Hf—Nd isotopic signature of veined pyroxenite-infiltrated peridotite as a possible source for E-MORB

G. Borghini<sup>a</sup>, E. Rampone<sup>b,\*</sup>, C. Class<sup>c</sup>, S. Goldstein<sup>c,d</sup>, Y. Cai<sup>c,\*\*</sup>, A. Cipriani<sup>c,e</sup>, A. W. Hofmann<sup>c,f</sup>, L. Bolge<sup>c</sup>

- <sup>a</sup> Dipartimento di Scienze Terra "Ardito Desio", University of Milano, via Botticelli 23, 20133 Milano, Italy
- <sup>b</sup> DISTAV, Univewrsity of Genova, corso Europa 26, 16132 Genova, Italy
- <sup>c</sup> Lamont Doherty Earth Observatory of Columbia University, Palisades, NY 10964, USA
- <sup>d</sup> Department of Earth and Environmental Sciences, Columbia University, Palisades, NY 10964, USA
- <sup>e</sup> Dip. Scienze Chimiche e Geologiche, Universita`di Modena e Reggio Emilia, Largo S. Eufemia 19, 41100 Modena, Italy
- f Max-Planck-Institut für Chemie, 55020 Mainz, Germany

### ARTICLE INFO

Editor: Catherine Chauvel

Keywords:
Pyroxenites
Melt-rock reaction
Alpine-Apennine ophiolites
Mantle peridotites
Lu-Hf isotopes
MORB source

### ABSTRACT

Pyroxenite-peridotite sequences from the External Liguride (EL) Jurassic ophiolites (Northern Apennines, Italy) consist of portions of fertile MORB mantle that were modified by deep melt infiltration and melt-peridotite reaction. They represent an excellent natural example of a MORB-like veined mantle including unmodified peridotite, pyroxenite layers and metasomatized peridotite. We carried out a spatially controlled Hf isotope study on these mantle sequences to investigate how the Nd and Hf isotopic systems are affected by pyroxenite emplacement and melt-peridotite interactions. Present-day Lu-Hf isotopic compositions of these lithologies show a large range of  $^{176}$ Lu/ $^{177}$ Hf and  $^{176}$ Hf/ $^{177}$ Hf ratios that are correlated with their Nd isotopic compositions. Pyroxenite-free peridotites delineate a Hf-Nd isotope array that corresponds to a Proterozoic age (> 1.5 Ga) which is likely related to the accretion to the subcontinental lithosphere of this mantle sector. Heterogeneous <sup>176</sup>Hf/<sup>177</sup>Hf isotopic compositions in pyroxenites mostly correlate with the significant variations of <sup>176</sup>Lu/<sup>177</sup>Hf ratios and reflect variable garnet abundance in the primary modal assemblage. Over time, the pyroxenites acquired a large range of eHf values, which encompass the global range of Hf-Nd isotopes in ocean ridge basalts. Infiltration of pyroxenite-derived melts led the host peridotite to acquire low Lu/Hf ratios with the consequent development of <sup>176</sup>Hf/<sup>177</sup>Hf ratios lower than in the unmodified peridotite, generating an equivalent of an enriched mantle component. This melt-peridotite interaction likely occurred during the pyroxenite emplacement 430 Ma ago, as confirmed by two Lu-Hf local pyroxenite-peridotite isochrons. The chemical and isotopic changes produced, over time, a spread of Hf-Nd isotopic signatures of the EL veined mantle, covering almost the entire range of published MORB compositions. Pyroxenite emplacement and local metasomatism of the host peridotites thus created Hf-Nd enriched mantle domains, making the EL veined mantle the first reported natural example of an enriched MORB-like mantle that formed through the combined effect of deep emplacement of pyroxenite and pyroxenite-peridotite interaction. The structure and isotopic characteristics of the EL veined mantle were used to model the isotopic compositions of melts produced by decompression melting of threecomponent heterogeneous mantle sources, providing an additional scenario to the generation of EMORB erupted at mid-ocean ridge settings. Our results emphasize the potential role of deep pyroxenite infiltration in modifying the host peridotites by interaction with pyroxenite-derived melts and creating heterogeneous mantle domains

E-mail addresses: elisabetta.rampone@unige.it (E. Rampone), cai@ldeo.columbia.edu (Y. Cai).

<sup>\*</sup> Corresponding author at: Dipartimento di Scienze della Terra, dell'Ambiente e della Vita (DISTAV), Università degli Studi di Genova, Corso Europa 26, I-16132 Genova, Italy.

<sup>\*\*</sup> Corresponding author.

### 1. Introduction

There is long-standing evidence that the mantle source of oceanic basalts is lithologically heterogeneous, including both refractory domains (residual peridotitic and/or harzburgitic oceanic and/or subcontinental lithospheric mantle), and enriched domains in the form of pyroxenite and/or eclogite lithologies (e.g. Hirschmann and Stolper, 1996). Such pyroxenites/eclogites may be remnants of subducted ocean crust (Allègre and Turcotte, 1986), or they may be formed by partial melts that infiltrate the peridotite and form veins (Sun and Hanson, 1975). These components were stretched, stirred, and sometimes melted in the asthenosphere to form a veined, heterogeneous mantle. The evidence for this veined mantle includes the chemical and isotopic variability of oceanic basalts (mid-ocean ridge basalts - MORBs and ocean island basalts - OIBs), the lithologic variability observed in exposed ophiolitic and oceanic mantle sections (e.g. pyroxenite occurrence) (e.g. Shimizu et al., 2016), as well as several experimental studies of partial melting of peridotite and pyroxenite lithologies (e.g. Stracke and Bourdon, 2009; Warren et al., 2009; Salters et al., 2011; Lambart et al., 2013; Lambart et al., 2016; Brunelli et al., 2018; Sanfilippo et al., 2019).

The quantitative role of pyroxenites in the MORB and OIB generation has been evaluated by different types of studies: studies based on natural samples, e.g. Mn, Ni contents in olivine phenocrysts in OIBs (Sobolev et al., 2005, 2007; Hezberg et al., 2016), melting degree estimates in oceanic peridotite-basalt associations pointing to the presence of a low-melting pyroxenite component in the mantle source (e.g. Brown and Lesher, 2014, 2016; Brunelli et al., 2018, U-series isotopes in oceanic basalts (Elkins et al., 2019); studies using experimental approaches (e.g. MORB eclogite – peridotite reaction, Mallik and Dasgupta, 2012, 2013); and numerical modeling studies (e.g. MELT-Px modeling of pyroxenite-peridotite melting, Lambart et al., 2016).

Moreover, recent studies (e.g. Sobolev et al., 2005; Herzberg, 2011; Lambart et al., 2012, Lambart et al., 2013, Lambart, 2017) have emphasized the important role of secondary (or "stage-2") pyroxenites, i.e. Mg-rich pyroxenites generated by reaction between peridotites and pyroxenite-derived melts, during the upwelling of veined mantle. Secondary pyroxenites can generate melts with similar major element compositions as peridotite melts, thus representing a hidden major element component (Lambart et al., 2009; Borghini et al., 2017). However, their inherited trace element signatures, in combination with their isotopic signatures, can preserve clues to their origin, as recycled oceanic crust and/or aged igneous lithospheric veins, and these signatures can be transferred to the oceanic basalts during melting. As the emplacement of pyroxenite layers within mantle peridotite may result in a significant mineralogical and/or chemical modification of the host mantle rocks (e.g. Bodinier et al., 1990, 2004; Pearson et al., 1993; Zanetti et al., 1996; Mukasa and Shervais, 1999), a crucial aspect of the occurrence of pyroxenite components in mantle sources, beyond their direct involvement in mantle melting, concerns the interaction between pyroxenite-derived melts and the surrounding mantle. Interactions between pyroxenite-derived melts and peridotites in creating re-fertilized "hybrid" heterogeneous mantle domains have been explored by a few studies (Lambart et al., 2012; Lambart et al., 2013; Borghini and Fumagalli, 2020). However, despite their importance, natural analogs of such "hybrid" domains within a MORB-like mantle are very rare and detailed studies are needed to characterize how the Nd and Hf isotopic systems are affected by pyroxenite emplacement and hybridization in MORB-mantle sections.

Over the last two decades, our knowledge on the Lu—Hf isotopic composition of the MORB mantle has expanded greatly owing to studies on peridotite, pyroxenite and basalt samples coming from oceanic settings (e.g. Stracke et al., 2011; Salters et al., 2011; Mallick et al., 2014; Byerly and Lassiter, 2014; Sanfilippo et al., 2019) and fossil analogs (e.g. Rampone and Hofmann, 2012; Montanini et al., 2012; Montanini and Tribuzio, 2015; Tilhac et al., 2016, 2020). In this study the terms "enriched" and "depleted", when applied to isotope ratios, represent the

effects of long-term incompatible element enrichment or depletion on present-day isotope ratios. Because low Lu/Hf and Sm/Nd ratios (and high Rb/Sr ratios) reflect incompatible element enrichment, low Nd-Hf (and high Sr) isotope ratios represent "enriched" sources, while high Nd-Hf (and low Sr) isotope ratios represent "depleted" sources. Robust Nd-Hf isotopic correlations observed in MORBs on a global scale has extended the MORB field towards highly depleted compositions (Salters et al., 2011), revealing significant contributions from refractory mantle domains. Moreover, extremely radiogenic Hf-isotopic compositions, plotting far from the OIB-MORB array, documented in abyssal and ophiolite peridotites (Stracke et al., 2011; Sanfilippo et al., 2019) suggest that the asthenospheric mantle may preserve portions of ancient, lithospheric melt residues (called ReLish for Refractory Lithosphere, Salters et al., 2011). Few studies have reported Hf and Nd isotopic compositions in mantle pyroxenites (Blichert-Toft et al., 1999; Pearson and Nowell, 2004; Bizimis et al., 2005; Montanini et al., 2012; Ackerman et al., 2016; Lu et al., 2018; Tilhac et al., 2020). Some pyroxenites show decoupled Hf-Nd isotope ratios towards more radiogenic Hf isotope compositions (e.g. Blichert-Toft et al., 1999; Bizimis et al., 2005; Tilhac et al., 2020). However, detailed isotopic investigations on pyroxenite-peridotite associations (i.e. also including host peridotites) are still missing. Hence, the role of pyroxenites in the isotopically heterogeneous mantle and the effect of their emplacement within mantle domains remain still unexplored.

A unique opportunity to study such domains is given by mantle peridotites and associated pyroxenites from the External Liguride (EL) ophiolites (Northern Apennines, Italy, Fig. 1a). The EL ophiolites are considered to represent sectors of oceanic lithosphere of the Jurassic Alpine Tethys Ocean formed in an ocean-continent transition setting (similar to present-day passive margins, like the Iberia margin; Rampone and Piccardo, 2000), and consist of Proterozoic exhumed subcontinental lithospheric mantle (Rampone et al., 1995; Snow et al., 2000) primarily associated with thinned continental crust. Some EL mantle sequences represent portions of asthenospheric MORB-like mantle (DM in terms of chemical and isotopic composition, Rampone et al., 1995) accreted to the subcontinental lithospheric mantle, which acquired heterogeneous chemical and, over time, isotopic signatures by infiltration of pyroxenites and peridotite modification via percolation of pyroxenite-related melts about 430 Ma ago (Borghini et al., 2013, 2020). This process likely occurred at high temperatures (above 1200 °C) and pressures (above 1.5 GPa) at the lithosphere-asthenosphere boundary (Hidas et al., 2021), i.e. at high-T mantle conditions. Therefore, EL can serve as a proxy for a MORB mantle source with peridotite veined by secondary pyroxenite, which could represent the heterogeneous mantle source invoked in MORB petrogenesis models (Lambart et al., 2012). Spatiallycontrolled elemental and Nd isotopic profiles in EL pyroxenites and host lherzolites point to significant enrichment in the host peridotites driven by reactive percolation of pyroxenite-derived melts (Borghini et al., 2013, 2020; Rampone et al., 2020). In this paper, we present Hf isotopic compositions of the same profiles, which demonstrate correlated Hf-Nd isotope ratios derived from the pyroxenite-peridotite interactions. Based on these results, we discuss their implications as enriched-MORB mantle sources.

### 2. Field and petrologic background

Ophiolites outcropping along the Alpine-Apennine (A-A) belts are remnants of the oceanic lithosphere of the Jurassic Alpine Tethys Ocean, a rather narrow basin opened in response to the Mesozoic divergence between Europa and Adriatic passive continental margins. In the A-A ophiolites, peridotites represent heterogeneous oceanic mantle mostly constituted of depleted mantle domains, similar to those created at modern oceanic ridges, and fertile mantle domains representing exhumed subcontinental mantle at extended continental margins (Rampone and Sanfilippo, 2021, and references therein). Among the latter, the EL ophiolites consist of several ultramafic bodies, mostly

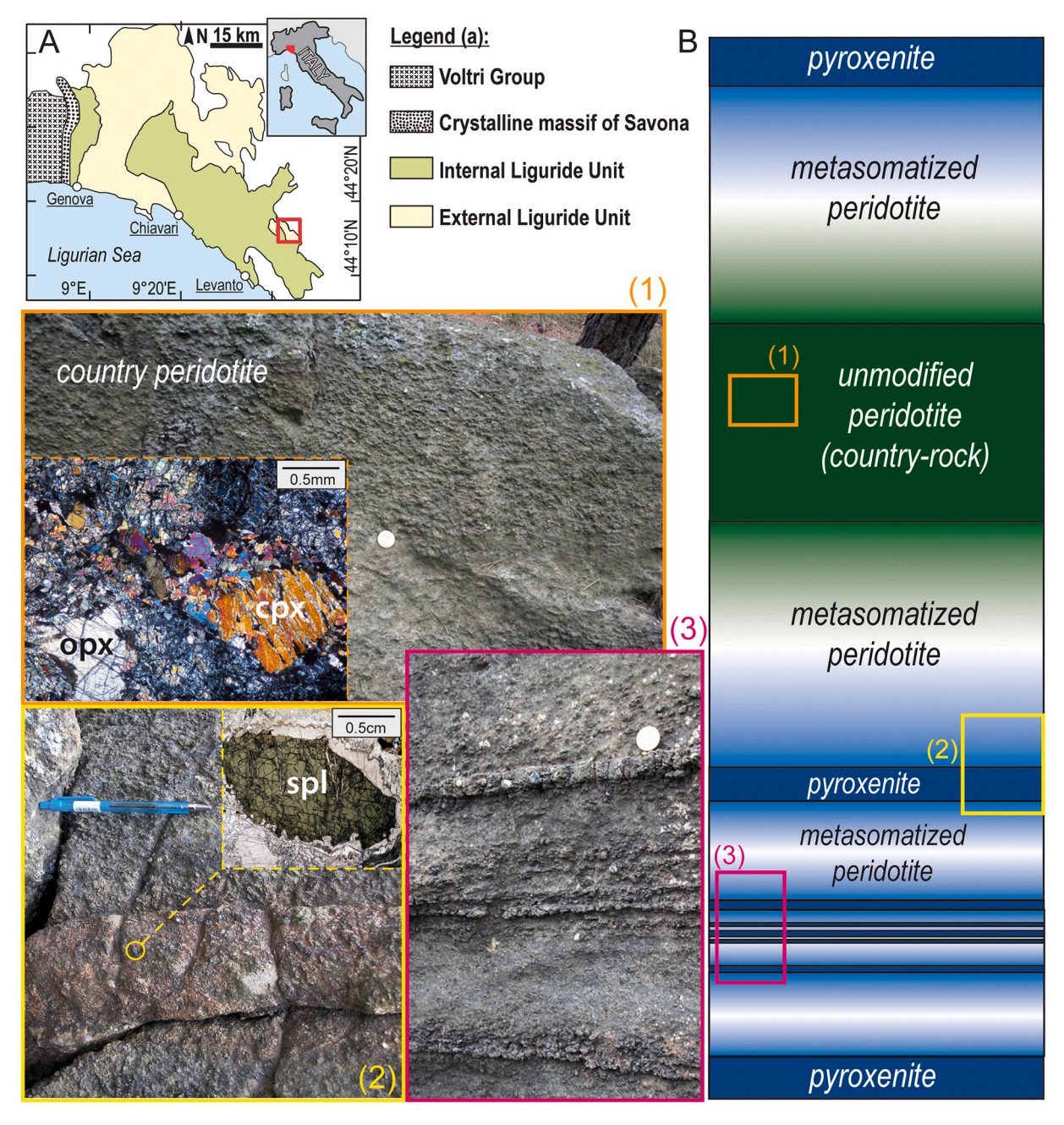


**Fig. 1.** (A) Schematic maps of the main tectonic units of the Northern Apennines. (B) Sketch of the veined pyroxenite-bearing mantle from the External Liguride Unit (EL), including cm-thick pyroxenite, metasomatized peridotite and unmodified peridotite (country rock). In the colored boxes we show: 1) the field occurrence of a country peridotite with pervasive tectonic foliation and photomicrograph of coarse pyroxene porphyroclasts that were partially replaced by a plagioclase-bearing fine-grained neoblastic assemblage, 2) a pyroxenite layer within the host peridotites and photomicrograph of a large green spinel in pyroxenite, and 3) thin (< 2 cm width) pyroxenite layers embedded in the mantle peridotite. (For interpretation of the references to colour in this figure legend, the reader is referred to the web version of this article.)

formed by fertile lherzolite associated to minor MOR-type basalts and rare gabbroic rocks, occurring as large olistoliths within Cretaceous sedimentary melanges obducted during the closure of the oceanic basin (e.g. Marroni et al., 2010). The subcontinental lithospheric nature of EL peridotites is indicated by their rather fertile composition, local dissemination of Ti-rich amphibole (e.g. Rampone et al., 1995; Vannucci et al., 1995), and diffuse occurrence of spinel and (minor) garnet pyroxenite layers (e.g. Montanini et al., 2006, 2012; Borghini et al., 2013, 2016). The EL peridotites of this study preserve highly depleted Nd–Sr–Os isotopic compositions that reflect very old depletion events (with Proterozoic ages; Rampone et al., 1995; Snow et al., 2000) and

suggest that these mantle sequences had a long residence time in the subcontinental lithosphere, without perturbation by melt percolation or partial melting. On the basis of chemical and isotopic compositions, Rampone et al. (1995) argued that this sector of EL mantle was derived by the accretion of MORB-type asthenospheric mantle to the lithosphere. After the lithospheric accretion, EL mantle experienced melt infiltration that generated pyroxenite layers and locally modified the peridotite (Borghini et al., 2013, 2016, 2020; Hidas et al., 2021). Hence, the MORB-like isotopic and chemical composition of the studied EL mantle sequences makes them a unique study case to investigate the chemical and isotopic modifications induced by pyroxenite

emplacement and related melt-rock reaction in a MORB-type mantle source (Borghini et al., 2013).

### 2.1. Origin of pyroxenites

In the EL pyroxenite-peridotite associations, the pyroxenites consist of spinel clinopyroxenites and websterites. They mostly occur as centimeter-scale layers (up to 10-15 cm) and less frequently as thicker layers (0.5-2 m) or lenses hosted by spinel lherzolites (Fig. 1). Borghini et al. (2016) studied the chemical features of the pyroxenites and discussed their origin. They showed that most pyroxenites still record chemical features inherited from a primary garnet-bearing assemblage, e.g. i) variable M- to HREE fractionation in bulk rocks, ii) high Sc, V, HREE contents in clinopyroxenes from spinel-rich domains of thicker layers which is indicative of precursor garnet-bearing domains. They estimated variable modal contents of garnet (11-40% by vol.) in the reconstructed primary assemblage. Accordingly, they inferred that pyroxenites originated by melt crystallization at relatively high-pressure conditions (1.6-2.4 GPa). Later, the primary garnet-bearing mineral associations were completely overprinted in a completely subsolidus recrystallization event by clinopyroxene-rich, spinel-facies assemblages, in which clinopyroxene largely inherited the trace element and isotopic composition of the pyroxenite bulk rocks (Borghini et al., 2013, 2016).

Moreover, Borghini et al. (2016) showed that the pyroxenites have major element compositions that are similar to silica saturated tholeiitic melts produced by reaction between MORB-eclogite partial melts and fertile peridotite (Mallik and Dasgupta, 2012). Based on this evidence, and the low Mg-values of their computed parental melts, they inferred that pyroxenites originated from melts produced by a hybrid [peridotite – silica-excess (SE) pyroxenite (or eclogite)] mantle source, which infiltrated and reacted with the overlying mantle, thus representing a natural proxy of second-stage (or secondary) pyroxenites associated with fertile lherzolites (see Borghini et al., 2016).

### 2.2. Evidence of pyroxenite-peridotite interaction

Borghini et al. (2013) documented textural and chemical evidence that are consistent with pyroxenite – peridotite interaction. They showed that the pyroxenites often exhibit orthopyroxene-enrichment at the peridotite-pyroxenite boundary, which is indicative of reaction between pyroxenite-derived melt and the adjacent wall-rock peridotite (e. g. Yaxley and Green, 1998). Borghini et al. (2013) also measured chemical and Sr—Nd isotopic profiles through the peridotite-pyroxenite boundary, which allowed them to distinguish the pyroxenite, the wall rock peridotite (up to 5 cm from the boundary), the host peridotite (between 5 and 10 cm) and the country peridotite (defined as peridotites that are free of pyroxenites at 1 m scale). They observed lower Mg-values and higher Al and Ca contents in the host and wall-rock peridotites compared to the country peridotites, and this indicated the local chemical modification of the peridotite by the interaction with pyroxenite-derived melts.

Hidas et al. (2021) performed electron backscatter diffraction (EBSD) analyses, phase maps and measurements of the crystallographic preferred orientation (CPO) of all minerals in a number of these peridotite-pyroxenite profiles. They observed a clear enrichment in clinopyroxene in the wall-rock peridotites relative to the country peridotites (far from pyroxenites), consistent with the chemical evidence of bulk CaO and  $Al_2O_3$  enrichment in wall-rock peridotites. Moreover, they found elongated clinopyroxene-rich domains in the wall-rock peridotites, oblique to the pyroxenite-peridotite contact, pointing to the presence of melt in the peridotite during deformation, and the synkinematic formation of pyroxenites. This is consistent with the preservation of geochemical gradients through the pyroxenite-peridotite boundary. On the contrary, pyroxenite-free country peridotites do not show any microstructural and/or chemical evidence of interaction with pyroxenite-derived melt, thus indicating that they were not affected by

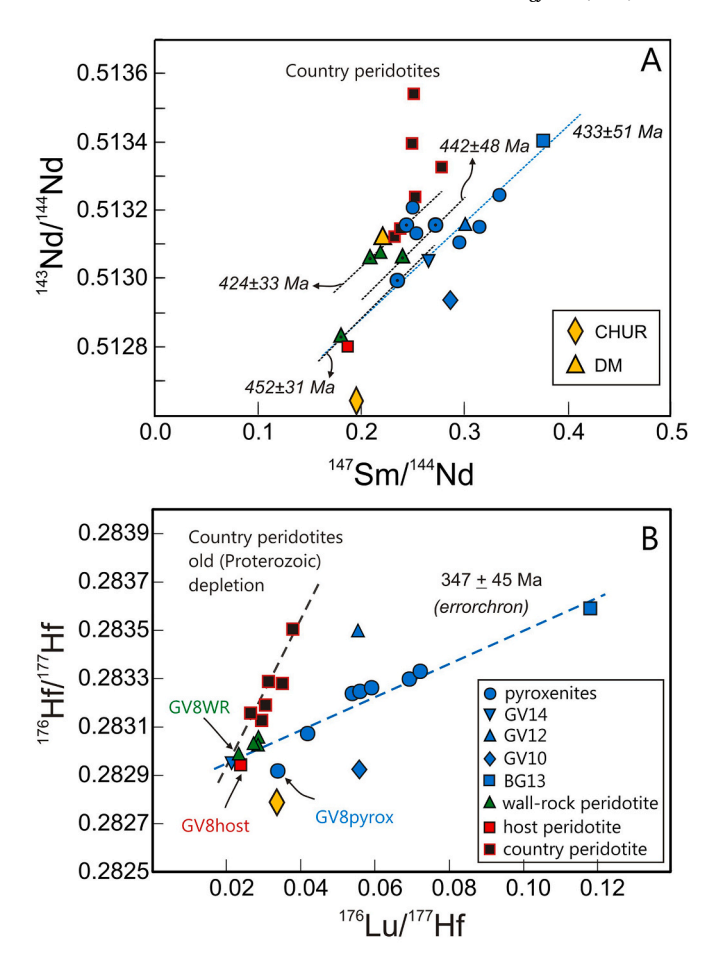


Fig. 2. Present-day  $^{143}$ Nd/ $^{144}$ Nd versus  $^{147}$ Sm/ $^{144}$ Nd (A) and  $^{176}$ Hf/ $^{177}$ Hf versus  $^{176}$ Lu/ $^{177}$ Hf (B) ratios in clinopyroxenes from External Liguride (EL) veined mantle. In (A) pyroxenites define an errorchron (blue dotted line) yielding an age of  $433 \pm 51$  Ma, which agrees well with the ages provided by three pyroxenite and wall-rock peridotite isochrons (black dashed lines connecting symbols with black dots inside) (Borghini et al., 2013). In (B) most of the pyroxenites together with wall-rock and host peridotites define an errorchron (blue dashed line) yielding an age of  $347 \pm 45$  Ma. Country peridotites reflect an old Proterozoic depletion (> 1 Ga). The Depleted Mantle (DM) and Chondritic Uniform Reservoir (CHUR) values for Nd isotopes are from Faure (1986). The CHUR value for Hf isotopes is from Bouvier et al. (2008). (For interpretation of the references to colour in this figure legend, the reader is referred to the web version of this article.)

### pyroxenite emplacement.

Borghini et al. (2013) investigated trace element variations in clinopyroxenes from three profiles across the pyroxenite-peridotite boundary. They found that wall-rock clinopyroxenes have systematically lower Sm/Nd ratios than clinopyroxenes in the country peridotites. Also, REE abundances in clinopyroxenes progressively increase away from the pyroxenite-peridotite boundary, which is consistent with reactive percolation of pyroxenite-derived melts within the peridotite at decreasing melt mass (Borghini et al., 2020). This melt-rock interaction has profound implications on the Nd isotopic signature of percolated peridotites. As shown in the <sup>147</sup>Sm/<sup>144</sup>Nd vs. <sup>143</sup>Nd/<sup>144</sup>Nd diagram (Fig. 2a), wall-rock and host peridotites are systematically shifted to lower Nd isotope ratios relative to the country peridotites, as a result of chemical interaction with pyroxenite-derived melts, combined with radiogenic ingrowth. Moreover, the three (wall-rock peridotite - pyroxenite) profiles provide a Paleozoic age (around 420-450 Ma), which could be considered the age of emplacement for the pyroxenites. This age is consistent with the age of the errorchon defined by all pyroxenites (Borghini et al., 2013, 2016). All the observations provided by previous

 Table 1

 Hf and Nd isotopic data for clinopyroxenes from External Liguride pyroxenites and peridotites.

| Sample            | R-t | Latitude       | Longitude   | Lu (ppm) | Hf (ppm) | <sup>176</sup> Lu/ <sup>177</sup> Hf | $^{176} Hf/^{177} Hf~(\pm 2\sigma \times 10^6)^a$ | εHf(0) | εHf(160) | εHf(430) | Sm (ppm) | Nd (ppm) | <sup>147</sup> Sm/ <sup>144</sup> Nd | $^{143}\text{Nd}/^{144}\text{Nd}~(\pm2\sigma\times10^6)^a$ | εNd(0) | εNd(160) | εNd(430) |
|-------------------|-----|----------------|-------------|----------|----------|--------------------------------------|---|--------|----------|----------|----------|----------|--------------------------------------|--|--------|----------|----------|
| BG1               | CP  | 44° 16′ 43.79″ | 9°47′52.28″ | 0.342    | 1.582    | 0.0307                               | $0.283189 \pm 05$                                 | 14.30  | 14.61    | 15.13    | 2.34     | 6.09     | 0.2319                               | $0.513119 \pm 08$  | 9.38   | 8.66     | 7.45     |
| BG6               | CP  | 44° 16′ 45.03″ | 9°47′38.94″ | 0.419    | 1.686    | 0.0353                               | $0.283279 \pm 04$                                 | 17.47  | 17.30    | 17.00    | 1.95     | 4.69     | 0.2520                               | $0.513236 \pm 09$  | 11.66  | 10.53    | 8.62     |
| BG13C             | CP  | 44° 16′ 45.93″ | 9°47′48.93″ | 0.300    | 1.351    | 0.0315                               | $0.283288 \pm 05$                                 | 17.78  | 18.00    | 18.39    | 2.12     | 4.75     | 0.2753                               | $0.513331 \pm 09$  | 13.51  | 11.91    | 9.20     |
| BG23              | CP  | 44°16′46.46″   | 9°47′46.64″ | 0.381    | 2.026    | 0.0267                               | $0.283156 \pm 04$                                 | 13.14  | 13.87    | 15.11    | 2.28     | 5.80     | 0.2375                               | $0.513143 \pm 07$  | 9.84   | 9.01     | 7.60     |
| BG23 <sup>b</sup> | CP  |                |             | 0.381    | 2.026    | 0.0267                               | $0.283161 \pm 06$                                 | 13.28  | 14.02    | 15.26    | _        | _        | _                                    | -  | _      | _        | _        |
| GV18              | CP  | 44° 16′ 15.86″ | 9°48′27.96″ | _        | _        | _                                    | _   | _      | _        | _        | 2.58     | 6.25     | 0.2489                               | $0.513394 \pm 05$  | 14.74  | 13.68    | 11.88    |
| ERS2-2            | CP  | 44°16′48.56″   | 9°47′42.88″ | 0.390    | 1.451    | 0.0381                               | $0.283501 \pm 05$                                 | 25.33  | 24.86    | 24.07    | 1.85     | 4.48     | 0.2495                               | $0.513538 \pm 06$  | 17.56  | 16.48    | 14.67    |
| ERS2-2b           | CP  |                |             | 0.390    | 1.451    | 0.0381                               | $0.283503 \pm 06$                                 | 25.41  | 24.94    | 24.15    | _        | _        | _                                    | -  | _      | _        | _        |
| MC7               | CP  | 44° 17′ 40.55″ | 9°45′32.48″ | 0.330    | 1.578    | 0.0297                               | $0.283126 \pm 04$                                 | 12.05  | 12.47    | 13.17    | _        | _        | _                                    | -  | _      | _        | _        |
| BG8W              | WR  | 44°16′44.32″   | 9°47′50.35″ | 0.307    | 1.513    | 0.0288                               | $0.283051 \pm 05$                                 | 9.42   | 9.92     | 10.79    | 2.16     | 5.95     | 0.2196                               | $0.513079 \pm 09$  | 8.56   | 8.09     | 7.30     |
| BG14W             | WR  | 44°16′44.15″   | 9°47′50.15″ | 0.346    | 1.788    | 0.0275                               | $0.283022 \pm 05$                                 | 8.38   | 9.02     | 10.12    | 2.28     | 5.28     | 0.2412                               | $0.513065 \pm 06$  | 8.34   | 7.43     | 5.90     |
| BG22W             | WR  | 44°16′44.69″   | 9°47′49.57″ | 0.353    | 1.743    | 0.0287                               | $0.283026 \pm 05$                                 | 8.51   | 9.03     | 9.91     | 2.15     | 6.22     | 0.2086                               | $0.513059 \pm 05$  | 8.22   | 7.98     | 7.57     |
| GV8W              | WR  | 44° 16′ 15.65″ | 9°48′27.76″ | 0.334    | 2.014    | 0.0236                               | $0.282981 \pm 05$                                 | 6.91   | 7.98     | 9.78     | 2.88     | 9.60     | 0.1814                               | $0.512834 \pm 06$  | 3.83   | 4.14     | 4.67     |
| GV8H              | HP  | 44° 16′ 15.65″ | 9°48′27.76″ | 0.295    | 1.741    | 0.0240                               | $0.282942 \pm 05$                                 | 5.56   | 6.58     | 8.30     | 3.50     | 11.38    | 0.1861                               | $0.512799 \pm 08$  | 3.14   | 3.36     | 3.73     |
| BG4               | Py  | 44°16′44.36″   | 9°47′49.08″ | _        | _        | _                                    | _   | _      | _        | _        | 1.86     | 4.51     | 0.2491                               | $0.513208 \pm 09$  | 11.12  | 10.05    | 8.24     |
| BG5               | Py  | 44°16′44.57″   | 9°47′48.64″ | 0.488    | 1.168    | 0.0593                               | $0.283262 \pm 05$                                 | 16.86  | 14.14    | 9.53     | 1.59     | 3.77     | 0.2545                               | $0.513131 \pm 09$  | 9.62   | 8.44     | 6.44     |
| BG13              | Py  | 44° 16′ 45.93″ | 9°47′48.93″ | 1.765    | 2.116    | 0.1184                               | $0.283592 \pm 04$                                 | 28.53  | 19.57    | 4.35     | 3.53     | 5.54     | 0.3845                               | $0.513412 \pm 06$  | 15.10  | 11.27    | 4.78     |
| BG13 <sup>b</sup> | Py  |                |             | 1.765    | 2.116    | 0.1184                               | $0.283592 \pm 06$                                 | 28.53  | 19.57    | 4.35     | _        | _        | _                                    | _  | _      | _        | _        |
| BG14P             | Py  | 44°16′44.15″   | 9°47′50.15″ | 0.465    | 1.220    | 0.0541                               | $0.283237 \pm 05$                                 | 16.00  | 13.83    | 10.16    | 1.99     | 4.43     | 0.2721                               | $0.513155 \pm 07$  | 10.08  | 8.55     | 5.94     |
| BG22P             | Py  | 44° 16′ 44.69″ | 9°47′49.57″ | 0.485    | 1.240    | 0.0555                               | $0.283246 \pm 05$                                 | 16.32  | 14.01    | 10.09    | 2.20     | 5.46     | 0.2435                               | $0.513156 \pm 05$  | 10.11  | 9.16     | 7.54     |
| GV8P              | Py  | 44° 16′ 15.65″ | 9°48′27.76″ | 0.477    | 1.987    | 0.0340                               | $0.282917 \pm 05$                                 | 4.68   | 4.64     | 4.56     | 3.67     | 9.35     | 0.2373                               | $0.512995 \pm 09$  | 6.97   | 6.17     | 4.82     |
| GV10              | Py  | 44° 16′ 15.86″ | 9°48′26.82″ | 0.839    | 2.126    | 0.0560                               | $0.282923 \pm 05$                                 | 4.88   | 2.51     | -1.50    | 2.32     | 4.89     | 0.2875                               | $0.512936 \pm 08$  | 5.82   | 3.97     | 0.83     |
| GV12              | Py  | 44° 16′ 15.95″ | 9°48′27.14″ | 0.229    | 0.585    | 0.0556                               | $0.283498 \pm 05$                                 | 25.23  | 22.90    | 18.96    | 0.80     | 1.59     | 0.3019                               | $0.513155 \pm 09$  | 10.08  | 7.93     | 4.30     |
| GV14              | Py  | 44° 16′ 15.95″ | 9°48′27.14″ | 0.236    | 1.530    | 0.0219                               | $0.282952 \pm 04$                                 | 5.90   | 7.14     | 9.25     | 2.78     | 6.30     | 0.2660                               | $0.513052 \pm 09$  | 8.07   | 6.65     | 4.24     |
| GV17              | Py  | 44° 16′ 28.53″ | 9°48′17.59″ | 0.514    | 1.732    | 0.0421                               | $0.283072 \pm 04$                                 | 10.15  | 9.26     | 7.74     | 2.39     | 4.88     | 0.2963                               | $0.513105 \pm 09$  | 9.10   | 7.07     | 3.63     |
| MC3               | Py  | 44° 17′ 38.25″ | 9°45′42.58″ | 0.946    | 1.932    | 0.0695                               | $0.283297 \pm 05$                                 | 18.10  | 14.31    | 7.87     | 2.64     | 4.79     | 0.3332                               | $0.513243 \pm 09$  | 11.81  | 9.02     | 4.31     |
| MC5               | Py  | 44° 17′ 37.54″ | 9°45′48.54″ | 1.242    | 2.433    | 0.0724                               | $0.283329 \pm 05$                                 | 19.25  | 15.15    | 8.18     | 2.73     | 5.23     | 0.3158                               | $0.513150\pm13$  | 9.99   | 7.55     | 3.44     |

R-t: Rock type; CP: country peridotite; WR: wall-rock peridotite; HP: host peridotite; Py: pyroxenite.

Nd isotopic data are from from Borghini et al. (2013).

Values used for εNd(t) calculations: 143Nd/144NdCHUR = 0.512638 and 147Sm/144NdCHUR = 0.1966 (Jacobsen and Wasserburg, 1980).

Values used for  $\epsilon$ Hf(t) calculations: 176Hf/177HfCHUR = 0.282785 and 176Lu/177HfCHUR = 0.0336 (Bouvier et al., 2008).

<sup>&</sup>lt;sup>a</sup> Internal precision.

<sup>&</sup>lt;sup>b</sup> Duplicates on different aliquots of cpx separates.

studies thus indicate that the pyroxenite-peridotite associations of the EL mantle sections represent E-MORB-type mantle domains composed of unmodified peridotite (pyroxenite-free "country" peridotite) veined by centimeter- to meter-length portions of pyroxenites and metasomatized host peridotite (Fig. 1b).

#### 3. Samples and methods

Lu—Hf isotopic compositions of our samples are reported in Table 1, together with Nd isotopic data from Borghini et al. (2013). They consist of: i) seven country peridotites, ii) three spatially controlled (wall-rock and/or host peridotite – pyroxenite) profiles (samples GV8H-GV8W-GV8P, BG14W-BG14P, BG22W-BG22P), nine additional pyroxenite samples.

Lu—Hf isotope analyses were performed on clinopyroxene (90-150 μm), separated by grinding, sieving, electromagnetic separation and handpicking under a microscope. Unleached concentrate weights were in the range of 244-1563 mg, and the largest samples were split into different aliquots before leaching, digestion and chemistry in order to avoid overloading the columns. We saved an aliquot of each sample for Lu/Hf determination before chemistry. Clinopyroxene separates were leached in three steps (5 min, 5 min in sonicator, 10 min in hot plate at 150 °C), using a solution of 5% HF + 6.2 M HCl. Dissolved samples were purified for Hf using Eichrom ® Ln resin following routine procedures (Cai et al., 2014). Hf-isotope ratios were measured on a Thermo-Scientific Neptune Plus Multi-Collector-Inductively-Coupled-Plasma-Mass-Spectrometry (MC-ICP-MS) at the Lamont-Doherty Earth Observatory of Columbia University. Potential interference of <sup>176</sup>Yb on <sup>176</sup>Hf was corrected using 172Yb/176Yb of 1.710815 and 175Lu/176Lu ratio of 37.61. Instrumental in-run mass fractionation was corrected using  $^{179}\mathrm{Hf}/^{177}\mathrm{Hf}=0.7325.$  An in-house Hf elemental standard made by Johnson-Matthey, with identical isotopic composition as JMC475, was used to bracket the unknowns. Unknowns were normalized to average <sup>176</sup>Hf/<sup>177</sup>Hf value of 0.28216 for Johnson-Matthey/JMC475. The external reproducibility of the standards was 13–17 ppm (2RSD) for the run sessions. BCR2 standards run as unknowns yielded 0.282876  $\pm$  13 (2 s, n = 5), which agrees well with published values (Jweda et al., 2016; Weis et al., 2007). Total procedural blanks were below 80 pg and thus no blank corrections were made. Lu and Hf concentrations were measured on a VG ExCell quadrupole ICP-MS at Lamont using the standard addition method on an aliquot of the leached and dissolved clinopyroxene separates for isotopes. The uncertainty on each element is about 2% (1RSD). <sup>176</sup>Lu/<sup>177</sup>Hf ratios were calculated starting from the Lu/Hf elemental ratio measured by ICP-MS by using the relation

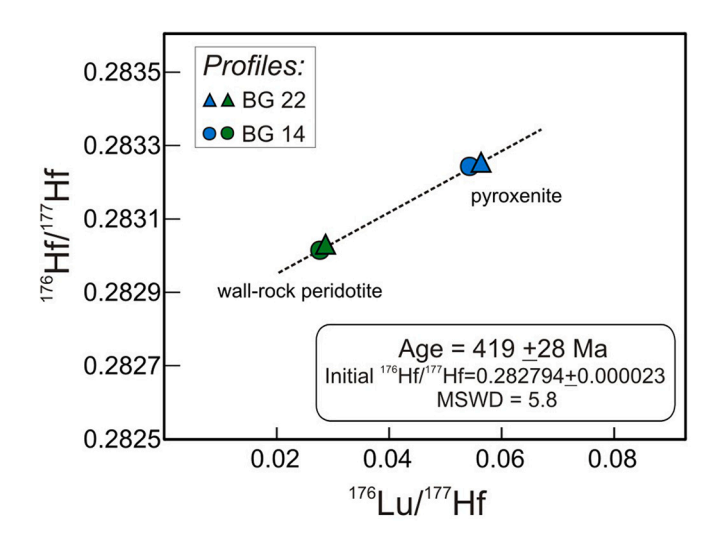


Fig. 3. Local isochron defined by present-day  $^{176}$ Hf/ $^{177}$ Hf versus  $^{176}$ Lu/ $^{177}$ Hf in clinopyroxenes from two spatially controlled pyroxenite – wall-rock peridotite profiles from EL veined mantle.

(sample ER-S2/2: 0.513538) also exhibits the highest  $^{176}$ Hf/ $^{177}$ Hf value (0.283501) coupled to a rather low  $^{176}$ Lu/ $^{177}$ Hf ratio (0.0381).

Pyroxenites show heterogeneous <sup>176</sup>Hf/<sup>177</sup>Hf ratios, mostly correlated with the large variations of <sup>176</sup>Lu/<sup>177</sup>Hf ratios (Fig. 2b). Consistent with the results of Sm-Nd isotopes, pyroxenite BG13, with the highest estimated garnet modal abundance in the reconstructed primary assemblage (40% of modal garnet; Borghini et al., 2016), exhibits the highest Hf isotopic values ( $^{176}$ Hf/ $^{177}$ Hf = 0.283592;  $^{176}$ Lu/ $^{177}$ Hf = 0.1184). Most pyroxenites cluster on an errorchron yielding an age of  $347 \pm 45$  Ma, which is much younger but still within uncertainty of the age obtained by Sm—Nd isotope data (433  $\pm$  51 Ma; Fig. 2a). Moreover, three wall-rock peridotite – pyroxenite pairs show "local" isochrons for the Sm-Nd system (Borghini et al., 2013) and two of those pairs define "local" isochrons in the Lu—Hf system yielding a consistent age (419  $\pm$ 28 Ma) (Fig. 3). As argued in Borghini et al. (2013), the reactive melt infiltration resulted in the resetting of Nd isotopes of the wall-rock peridotite to the values of the infiltrating pyroxenite. This also caused variable lowering of the Sm/Nd ratios that generated the wall-rock peridotite - pyroxenite "local" isochrons. The preservation of Lu-Hf isotope linear correlation in two of three pyroxenite-peridotite profiles is

 $^{176}$ Lu/ $^{176}$ Hf = (Lu/Hf) × 0.0001478728 × ( $^{176}$ Hf/ $^{177}$ Hf x175.941406 + 910.107822).

### 4. Results

Present-day Lu—Hf isotopic compositions of the peridotites and pyroxenites are presented in Table 1 and shown in Fig. 2b. Consistent with the Sm—Nd isotopes, pyroxenites, wall-rock and host peridotites (adjacent to pyroxenite layers) define a rather broad range of  $^{176} {\rm Lu}/^{177} {\rm Hf}$  and  $^{176} {\rm Hf}/^{177} {\rm Hf}$  ratios. In particular, wall-rock and host peridotites (adjacent to pyroxenite layers) define a narrow range, mostly confined at lower  $^{176} {\rm Lu}/^{177} {\rm Hf}$  and  $^{176} {\rm Hf}/^{177} {\rm Hf}$  ratios relative to the country peridotites that, instead, show a moderate range of  $^{176} {\rm Hf}/^{177} {\rm Hf}$  ratios (up to high values) for a rather narrow range of low  $^{176} {\rm Lu}/^{177} {\rm Hf}$  ratios (Fig. 2b). According with its extremely depleted Sr isotopic composition ( $^{87} {\rm Sr}/^{86} {\rm Sr} = 0.701736$ , Rampone et al., 1995; Borghini et al., 2013), the country peridotite with the highest  $^{143} {\rm Nd}/^{144} {\rm Nd}$  ratio

presumably related to the same reactive melt percolation event (see discussion below). Profile GV8 does not provide any Hf-isotope age because the  $^{176}\mathrm{Hf}/^{177}\mathrm{Hf}$  and  $^{176}\mathrm{Lu}/^{177}\mathrm{Hf}$  ratios of pyroxenite GV8 deviate from the alignment defined by most of pyroxenites (Fig. 2b). This mismatch could be due to the occurrence of an additional phase able to fractionate Lu/Hf ratio or a bias in pyroxenite sampling.

Two pyroxenite samples (GV12 and GV10) do not fall on the errorchron; they are characterized by higher and lower  $^{176}$ Hf/ $^{177}$ Hf values respectively, at similar  $^{176}$ Lu/ $^{177}$ Hf ratios. Pyroxenite GV10 also has the lowest  $^{143}$ Nd/ $^{144}$ Nd ratio among pyroxenites and does not conform to the Sm—Nd errorchron defined by most pyroxenite samples, whereas pyroxenite GV12 plots on this array (Fig. 2a).

Fig. 4 shows the initial εNd vs. εHf values of the pyroxenites, wallrock, host and country peridotites, computed at 160 Ma (i.e. the

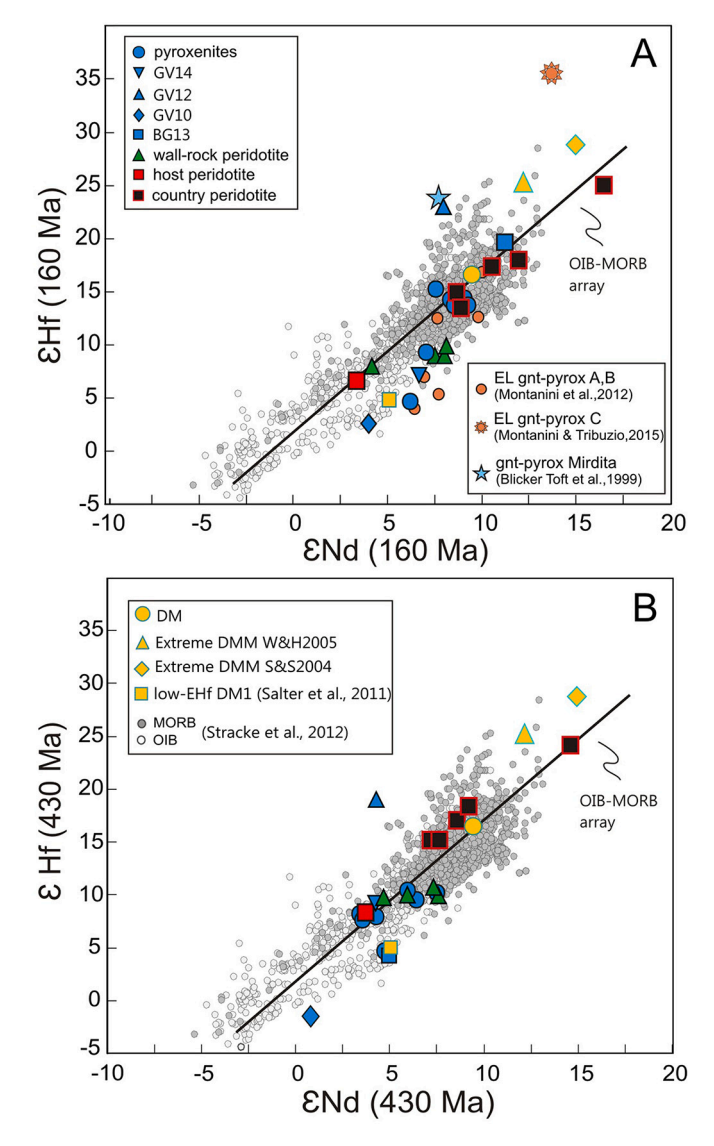


**Fig. 4.** Initial εNd versus εHf values computed at 160 (A) and 430 (B) Ma (see the text for explanation) of the pyroxenites and peridotites from EL veined mantle. Compilation of MORB and OIB, and the MORB-OIB array are from Stracke (2012). Also reported are the εNd-εHf values of the Depleted Mantle (Faure, 1986; Griffin et al., 2000), the Extreme Depleted MORB Mantle (DMM; after Salters and Stracke, 2004 and Workman and Hart, 2005), and the low-εHf Depleted Mantle (Salters et al., 2011). In (A) we also show for comparison the data of garnet pyroxenites from the External Liguride (Montanini et al., 2012; Montanini and Tribuzio, 2015) and Albanian ophiolites (Blichert-Toft et al., 1999).

inferred age of ocean floor exhumation of this mantle unit; Fig. 4a) and 430 Ma (i.e. the inferred age of pyroxenite emplacement at mantle conditions; Fig. 4b, Borghini et al., 2016). Specifically, the ε-values computed at 160 Ma should provide a portrait of the isotopic heterogeneity recorded by the External Liguride (EL) mantle sector at the time of its oceanic exposure, that is, in a geodynamic context analogous to modern oceanic mantle. In Fig. 4a we also report, for comparison, i) the bulk-rock compositions of garnet pyroxenites from EL (after Montanini et al., 2012 and Montanini and Tribuzio, 2015) and Albanian ophiolites (after Blichert-Toft et al., 1999); ii) the estimated compositions of the Extreme Depleted MORB Mantle (DMM; after Salters and Stracke, 2004 and Workman and Hart, 2005) and the enriched low-εHf Depleted Mantle (low εHf DM1 after Salters et al., 2011); and iii) a compilation of MORB-OIB compositions by Stracke (2012).

In the εNd vs. εHf diagram of Fig. 4a (160 Ma values), EL peridotites

and pyroxenites define an overall positive correlation, which covers almost the entire range of MORB variations. The pyroxenites define a large range of EHf values, including both enriched and very depleted Hf isotopic compositions, similar to most EL garnet pyroxenites from previous studies (Montanini et al., 2012; Montanini and Tribuzio, 2015). Pyroxenite GV12 displays a high εHf (160 Ma)-value and Nd and Hf isotopic ratios deviate from the terrestrial array (Vervoort et al., 1999), in a manner that is similar to the Albanian garnet pyroxenite. An extremely depleted Hf isotopic composition that is also off the Nd-Hf terrestrial array was reported by Montanini and Tribuzio (2015) for an EL garnet pyroxenite (type C) (Fig. 4a). Pyroxenite GV10 exhibits the lowest εNd-εHf values, which plots close to the low-εHf Depleted Mantle estimate of Salters et al. (2011). The country peridotites with higher EHf plot on the more depleted side of the MORB-OIB array, extending towards the Extreme Depleted MORB mantle estimates (Fig. 4a). On the other hand, melt-infiltrated peridotites (wall-rock and host) are shifted towards lower EHf-ENd values relative to the country peridotites. Together with some pyroxenites, they define a cluster around the lowεHf Depleted Mantle composition, at the enriched end of the MORB field (Fig. 4a).

The  $\epsilon$ Hf- $\epsilon$ Nd values of the pyroxenites and the peridotites calculated at 430 Ma (i.e. the age of pyroxenite formation) are reported in Fig. 4b. The country peridotites still exhibit a large range of variation at the depleted end of the MORB-OIB array. Remarkably, most pyroxenite samples (including BG13) and the melt-infiltrated (wall-rock and host) peridotites define a narrow variation, which clusters at relatively low  $\epsilon$ Hf- $\epsilon$ Nd values, close to the low- $\epsilon$ Hf DM estimate (Salters et al., 2011). Pyroxenites GV12 and GV10 still are the exceptions, plotting at higher  $\epsilon$ Hf (GV12) and lower  $\epsilon$ Hf- $\epsilon$ Nd values (GV10) with respect to the cluster defined by pyroxenites and melt-infiltrated peridotites (Fig. 4b).

### 5. Discussion

The EL peridotites and pyroxenites display significant isotopic variabilities, in terms of both Nd and Hf isotopic ratios (Fig. 2). The Hf and Nd isotopic variations are loosely correlated, and they cover almost the entire MORB-OIB array in the  $\epsilon$ Hf- $\epsilon$ Nd diagram of Fig. 4. Moreover, the similarity of Nd—Hf isotopic compositions computed at 430 Ma (see Fig. 4b) in most pyroxenites and metasomatised (wall-rock and host) peridotites, as well as their significant shift towards Enriched-MORB signatures with respect to the pristine (country) peridotites, point to the key role of pyroxenite emplacement in causing the observed Hf isotopic changes in this mantle section. In order to properly understand the observed Lu—Hf isotopic heterogeneity, first we need to establish the chemical and isotopic signature of the EL mantle before pyroxenite emplacement and discuss the Lu—Hf elemental behaviour in both the peridotites and the pyroxenites.

## 5.1. Nd—Hf isotopic variability in country peridotites: ancient lithospheric accretion

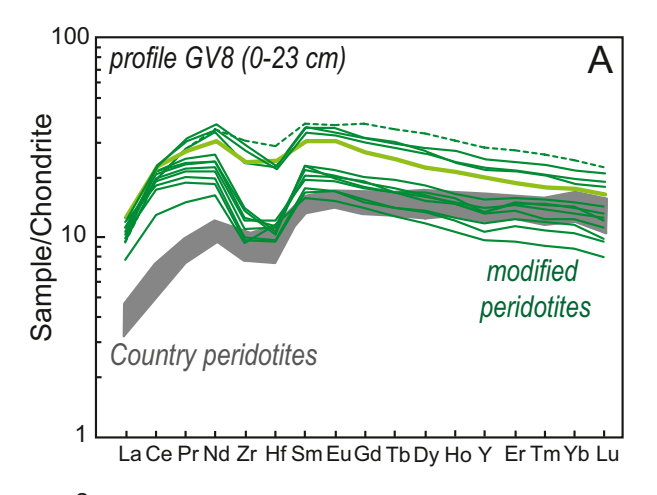
The country peridotites define a much steeper trend in Lu—Hf and Sm—Nd isochron plots with respect to the trend defined by most pyroxenites and modified peridotite (wall-rock and host) (Fig. 2b). This further corroborates our previous conclusion (Borghini et al., 2013, 2020) on the basis of chemical and Sr—Nd isotopic compositions that the pyroxenite emplacement did not affect these peridotites. In particular, the country peridotite ERS2/2 shows very high <sup>143</sup>Nd/<sup>144</sup>Nd and <sup>176</sup>Hf/<sup>177</sup>Hf ratios. Rampone et al. (1995) and Borghini et al. (2013) also documented a very low <sup>87</sup>Sr/<sup>88</sup>Sr value (0.70175) for this peridotite sample. Rampone et al. (1995) interpreted the extremely depleted Sr—Nd isotopic composition measured in the country peridotite ERS2/2 as the result of a long residence time in the subcontinental mantle. Sr and Nd model ages, calculated assuming both CHUR and DM mantle sources, range between 2.4 Ga and 780 Ma, with the 1.2 Ga Sr age and the 780 Ma Nd age potentially representing minimum ages of

differentiation (Rampone et al., 1995). In agreement with the preservation of highly depleted Nd—Sr isotopic compositions, very ancient Os model ages (~1.6 Ga) for this EL peridotite further support its long isolation at lithospheric conditions (Snow et al., 2000). Similar isotopic compositions were documented in peridotites from the Lanzo North ultramafic massif and considered as the evidence of a long-term (>0.5 Ga) depletion and a subcontinental origin of this peridotite body (Bodinier et al., 1991).

Hf isotope data of this study confirm the depleted isotopic signature of ERS2/2 peridotite ( $^{176}\mathrm{Hf}/^{177}\mathrm{Hf}=0.28350,$  combined with low  $^{176}\mathrm{Lu}/^{177}\mathrm{Hf}$  ratio =0.0381), in agreement with the results of Sr and Nd isotopes. Moreover, the country peridotites define an array again indicating Proterozoic ages (>1.5 Ga). Therefore the EL mantle, prior to pyroxenite emplacement, had the chemical and Sr-Nd-Hf-Os isotopic characteristics of an ordinary DM-like asthenospheric mantle accreted at lithospheric environment since very ancient, likely Proterozoic, times.

### 5.2. Elemental Lu/Hf behaviour in peridotites: the effect of melt/rock interaction

Lu—Hf isotopic compositions of clinopyroxenes in the pyroxenite-bearing peridotites clearly indicate that the observed isotopic variations are related to the presence of pyroxenites. Reactive percolation of pyroxenite-derived melts caused chemical modifications in the host peridotites as indicated by trace element chemical gradients that are



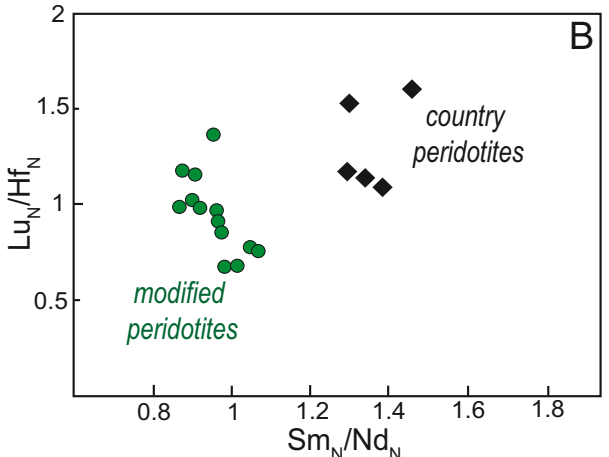


Fig. 5. Chondrite-normalized REE, Zr, Hf and Y patterns (A) and  $Lu_N/Hf_N$  versus  $Sm_N/Nd_N$  (B) of clinopyroxene porphyroclasts in the wall-rock and host (modified) peridotites from profile GV8, compared with the field defined by EL country peridotites (Borghini et al., 2020). Data are from Borghini et al. (2020). Normalizing values are from Anders and Grevesse (1989).

perpendicular to the pyroxenite-peridotite contacts (Borghini et al., 2013, 2020). Chemical and microstructural effects of melt percolation is limited to about 20 cm of host peridotite whereas country peridotites (sampled at more than 2 m from pyroxenite) show no chemical evidence for interaction with pyroxenite-derived melt or other melt/fluid metasomatism (Hidas et al., 2021). In order to understand the magnitude and extent of the chemical changes caused by pyroxenite-derived melts in the peridotites, Borghini et al. (2020) analyzed a 23 cm long profile from the edge of pyroxenite GV8 (5 cm thick) to the host peridotites. Fig. 5a reports the normalized trace element compositions (REE plus Zr and Hf) of clinopyroxenes in wall-rock and host (modified) peridotites of this profile and compares them to the compositional field defined by the clinopyroxenes in the country peridotites. Overall, the clinopyroxenes in the modified peridotites exhibit higher LREE, Zr, Hf contents and MREE/ HREE ratios. Moreover, the clinopyroxenes in the melt-infiltrated peridotites display markedly lower Sm/Nd ratios, and to a lesser extent, Lu/ Hf ratios, with respect to the clinopyroxenes in the country peridotites (Fig. 5b). The lower Lu/Hf ratio in wall-rock clinopyroxenes resulted from the decrease of HREE contents, caused by equilibration with percolating melts having a M- to HREE fractionated signature, similar to Enriched-MORB compositions (illustrated in Fig. 15b in Borghini et al., 2016, reporting the compositions of computed melts in equilibrium with the lowest wall-rock clinopyroxenes in the three profiles). Using trace element numerical modeling, Borghini et al. (2020) showed that chemical modification of melt-infiltrated peridotites (towards lower Sm/Nd and Lu/Hf ratios) can result from reactive (pyroxene producing, olivine dissolving) percolation of pyroxenite-derived melts (from the vein into the adjacent peridotite) at decreasing melt mass (i.e. at decreasing porosity, from 0.3 to 0.01), combined with chromatographic fractionation.

Infiltration of pyroxenite-derived melts, thus, effectively expanded the trace element enriched domains in the host mantle peridotites to be at least four times larger in size than the thickness of the pyroxenite itself. Such metasomatized mantle domains were modified in terms of elemental (Lu/Hf and Sm/Nd elemental ratios) and Nd—Hf isotopic compositions (i.e.  $\epsilon$ Nd- $\epsilon$ Hf values at 430 Ma in Fig. 4b). Over time, such chemical and isotopic changes resulted in the significant spread of Hf—Nd isotopic signatures observed in the EL peridotites (i.e.,  $\epsilon$ Nd- $\epsilon$ Hf values at 160 Ma, which is the age of oceanic emplacement, Fig. 4a), thereby covering almost the entire range of published MORB compositions. Moreover, this process generated an enriched mantle component discussed below.

## 5.3. Elemental Lu/Hf behaviour in pyroxenites: the effect of a garnet-bearing primary mode

In-situ trace element investigations combined with microstructural study of the pyroxenite layers have shown heterogeneous compositions in clinopyroxenes in relation to different mineralogical domains resulting from the inferred primary garnet-bearing mode. In some pyroxenite samples, systematic chemical zonation of HREE, Sc and V contents, with high values observed in spinel-rich domains and low concentrations in pyroxene-rich domains, have been ascribed to early garnet- and pyroxene-rich domains, respectively (Borghini et al., 2016). In Fig. 6a the normalized REE, Zr and Hf compositions of average clinopyroxene also show high variability among the different samples that mirror the trace element compositions of corresponding pyroxenite bulk rocks (Fig. 6b). This indicates that the spinel-facies clinopyroxene, due to complete replacement of the primary garnet-bearing mineral assemblage by subsolidus recrystallization, inherited the trace element signature of the pyroxenite bulk rocks. This is supported by the good correlations of  $\text{Lu}_N/\text{Hf}_N$  and  $\text{Sm}_N/\text{Nd}_N$  between bulk-rock and clinopyroxene separates (Supplementary Fig. 2). Accordingly, the large variability in the MREE-HREE fractionation (Fig. 6a), likely reflects variable garnet modal abundances in the primary mineral assemblages, consistent with their origin as melt segregates (Borghini et al., 2016). Results of mass balance calculation suggested that pyroxenites showing bulk compositions with high HREE content and/or enrichment of HREE over the MREE likely carried the highest garnet modal abundance (Borghini et al., 2016). Interestingly, pyroxenite GV12 shows significantly depleted LREE to MREE patterns that are also characterized by a marked negative Hf anomaly (Fig. 6a,b).

Fig. 7 compares the Lu<sub>N</sub>/Hf<sub>N</sub> versus Sm<sub>N</sub>/Nd<sub>N</sub> of average clinopyroxenes (analyzed in-situ by LA-ICP-MS), bulk rocks and clinopyroxene separates (solution ICP-MS, see Methods above). Overall, the Lu<sub>N</sub>/Hf<sub>N</sub> and Sm<sub>N</sub>/Nd<sub>N</sub> ratios are positively correlated while the Lu<sub>N</sub>/Hf<sub>N</sub> ratios define a larger range relative to the Sm<sub>N</sub>/Nd<sub>N</sub> ratios (Fig. 7). Accordingly, samples with more HREE-enriched bulk-rock and clinopyroxene compositions (Fig. 6a,b) show the highest Lu<sub>N</sub>/Hf<sub>N</sub> and Sm<sub>N</sub>/Nd<sub>N</sub> values (Fig. 7). These pyroxenites presumably contained relatively high garnet modal amounts in the primary mineral assemblage, as supported by mass balance modeling (Borghini et al., 2016). The good correlation shown by Lu<sub>N</sub>/Hf<sub>N</sub> and Sm<sub>N</sub>/Nd<sub>N</sub> ratios (Fig. 7b,c) further suggests that the clinopyroxene separates are representative of the bulk rocks (see also Supplementary Fig. 2). On the other hand, the scattering of some pyroxenite data in Fig. 7a is presumably related to the extreme trace element variability shown by clinopyroxene analyses by in-situ LA-ICP-MS observed in each sample (Borghini et al., 2016).

### 5.4. Significance of Nd—Hf isotopic variability in pyroxenites

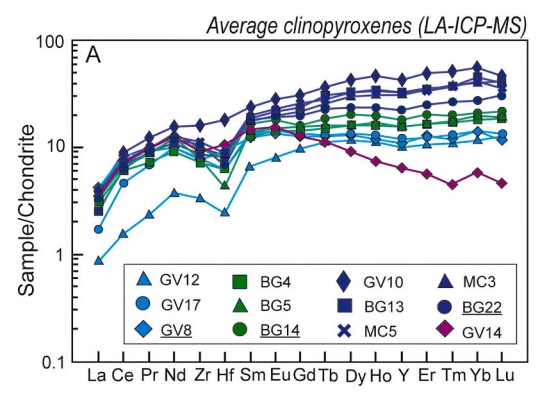
As shown in Fig. 7, the correlations of Lu<sub>N</sub>/Hf<sub>N</sub> and Sm<sub>N</sub>/Nd<sub>N</sub> ratios measured in single clinopyroxenes (in-situ LA-ICP-MS analyses), bulk rocks and clinopyroxene separates (see above) of pyroxenites mostly reflect the primary modal assemblage. In particular, the initial garnet modal abundance determines the variability of Lu<sub>N</sub>/Hf<sub>N</sub>, with the highest and lowest values shown by pyroxenite BG13 and GV14, respectively. Over time the variability in the Lu/Hf and Sm/Nd ratios resulted in high variability of the corresponding isotopic ratios, with pyroxenite BG13 showing the highest <sup>176</sup>Lu/<sup>177</sup>Hf (and <sup>147</sup>Sm/<sup>144</sup>Nd) and GV14 the lowest <sup>176</sup>Lu/<sup>177</sup>Hf (and one of the lowest <sup>147</sup>Sm/<sup>144</sup>Nd) ratios (Fig. 2). Most pyroxenites show a small range of Hf-Nd isotopic compositions at 430 Ma, the age of their emplacement (Fig. 4b). This suggests that the initial (430 Ma) Hf-Nd isotopic composition of pyroxenites reflect the isotopic signature of the infiltrating melts. This is reasonable because pyroxenite veins represented melt injections focused into conduits parallel to the mantle foliation that reacted with the host peridotites exclusively at the pyroxenite-peridotite contact (Hidas et al., 2021). Alternatively, they could have resulted from mixing between the infiltrating melt and the host peridotite, but this is not supported by the variability of the bulk major element chemistry and the correlation

between bulk composition and thickness of the pyroxenite layers (Borghini et al., 2016).

As a result of variable initial element ratios and radioactive decay since then, the pyroxenites acquired Hf—Nd isotopic compositions that at 160 Ma cover a large portion of the OIB-MORB mantle array (Fig. 4a). Significantly, these results demonstrate that pyroxenites in a single mantle sector can represent both depleted and enriched isotopic components, depending on their primary mineral assemblages, most importantly the modal abundance of garnet.

Samples GV12 and GV10 have initial  $\epsilon$ Hf and  $\epsilon$ Nd values that scatter from the pyroxenite Hf-Nd isotope cluster observed in Fig. 4b. They plot above and below the <sup>176</sup>Hf/<sup>177</sup>Hf and <sup>176</sup>Lu/<sup>177</sup>Hf trend defined by other pyroxenites, respectively (Fig. 2b). Pyroxenite GV12 has more radiogenic initial εHf at εNd similar to other pyroxenites, thus plotting above the MORB-OIB mantle array (Fig. 4b). In contrast, GV10 pyroxenite shows initial  $\epsilon$ Hf and  $\epsilon$ Nd both shifted towards enriched values and plotting slightly below the mantle array (Fig. 4b). Similar Hf-Nd isotopic decoupling has been commonly documented in pyroxenites from ultramafic massifs (Blichert-Toft et al., 1999; Pearson and Nowell, 2004; Montanini and Tribuzio, 2015; Ackerman et al., 2016; Varas-Reus et al., 2018; Tilhac et al., 2020). Montanini and Tribuzio (2015) attributed the highly radiogenic Hf isotopic compositions observed in their type-C garnet pyroxenite to a MORB-type troctolite protolith with high timeintegrated Lu/Hf ratios (see data reported in Fig. 4a). Alternatively, the Hf-Nd isotopic decoupling towards more radiogenic EHf could be explained as the result of melt-rock interaction with old depleted lithospheric mantle that had high time-integrated Lu/Hf ratios (Bizimis et al., 2005; Ackerman et al., 2016; Tilhac et al., 2020). Montanini and Tribuzio (2015) documented initial (160 Ma) εHf and εNd plotting below the mantle array in type A and B garnet pyroxenites. They inferred that the Hf-Nd decoupling was generated by the recycling of ancient long-lived gabbroic oceanic crust with low time-integrated Lu/ Hf ratios (Stracke et al., 2003), as previously suggested for some garnet pyroxenites from Beni Bousera ultramafic massif (Pearson and Nowell, 2004). Alternatively, initial εHf-εNd correlations towards low values observed in some pyroxenites have been considered to reflect the involvement of recycled oceanic sediments in the source of their parental melts (Pearson and Nowell, 2004; Ackerman et al., 2016).

Pyroxenite GV12 shows some differences in field occurrence and petrographic features relative to the other studied pyroxenites; it occurs as a thick lens rather than a thin layer and is characterized by (Al-rich spinel + clinopyroxene) clusters within a clinopyroxene-rich matrix (Borghini et al., 2016). Similar to type-C garnet pyroxenite of Montanini and Tribuzio (2015), GV12 is a clinopyroxenite that plots on the silicapoor side of the Fo-CaTs-Qtz-Di projection. Moreover, low REE



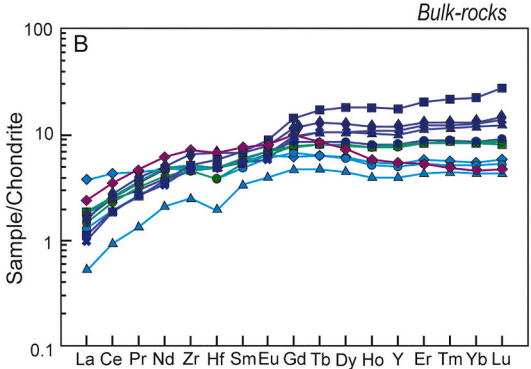


Fig. 6. Chondrite-normalized REE, Zr, Hf and Y patterns of average clinopyroxene porphyroclasts (A) and bulk-rocks (B) of the studied pyroxenites. Pyroxenite samples belonging to pyroxenite-peridotite profile are underlined. Data are from Borghini et al. (2016). Normalizing values are from Anders and Grevesse (1989).

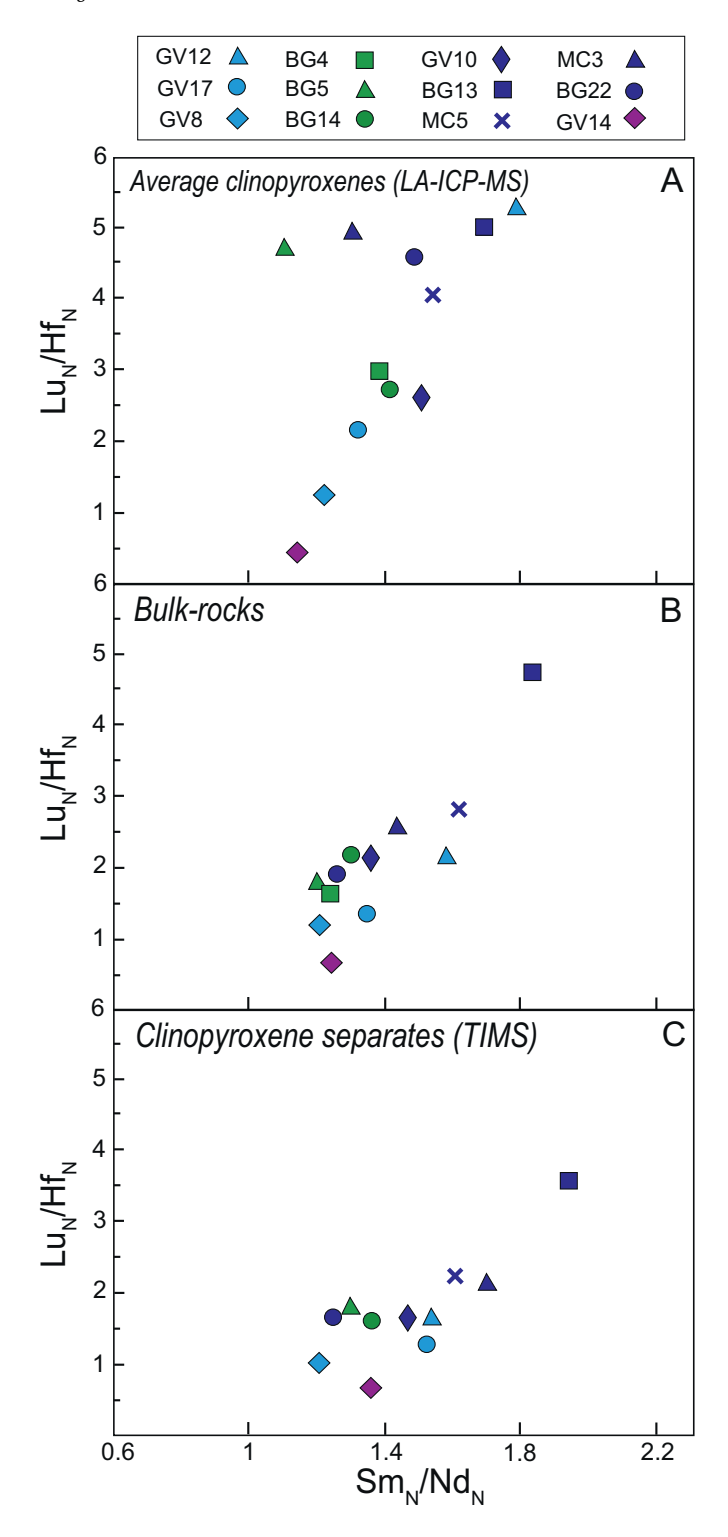


Fig. 7.  $Lu_N/Hf_N$  versus  $Sm_N/Nd_N$  of (A) average clinopyroxenes (analyzed insitu by LA-ICP-MS), (B) bulk rocks, and (C) clinopyroxene separates from the studied pyroxenites (data from Borghini et al., 2016).

abundances and the strong LREE-HREE fractionation shown by GV12 bulk rock and clinopyroxenes (Fig. 6) suggest that this pyroxenite might be residual in nature, although it has the lowest bulk  $X_{Mg}$  [molar Mg/ (Mg + Fe<sup>2+</sup><sub>tot</sub>)] (Borghini et al., 2016). Therefore, we cannot rule out that GV12 pyroxenite had a different origin with respect to the other studied pyroxenites, possibly related to the direct involvement of recycled crustal component, as documented in neighboring EL mantle sequences (Montanini and Tribuzio, 2015). Conversely, pyroxenite GV10

shares similar field, petrographic and chemical features with the other samples, therefore its Hf—Nd isotopic scattering remains poorly understood.

### 5.5. Origin of Enriched MORB mantle source by pyroxenite-peridotite interaction

Consistent with the findings based on Sm—Nd isotopes (Borghini et al., 2013), our new results show that the interaction between DM-like peridotite and pyroxenite-derived melt resulted in a decrease in Lu/Hf ratios and  $\epsilon$ Hf values in the melt-infiltrated peridotites ( $\epsilon$ Hf = 5–8, Fig. 4b). Pyroxenite emplacement induced a local metasomatism into the host peridotites, thus creating Hf—Nd enriched mantle domains, with compositions that resemble the estimated low- $\epsilon$ Hf DM (Salters et al., 2011). As such, this study presents the first reported natural example of an enriched MORB-like mantle that formed through the combined effect of deep emplacement of pyroxenite and interaction between pyroxenitic melt and ambient peridotite.

Although the EL peridotites represent exposed subcontinental lithospheric mantle, similar to modern passive margin peridotites (Rampone et al., 1995; Marroni et al., 1998), their MORB isotopic composition and DM-type fertile chemical signature indicate that they were formed by lithospheric accretion of ordinary asthenospheric mantle (Rampone et al., 1995; Borghini et al., 2013). Moreover, the enriched signatures of melts that generated the pyroxenite layers and metasomatized the host peridotites make the studied mantle sequences potential examples of EMORB mantle sources. Sampling of EMORBs along ridge segments far from plumes (e.g. Donnelly et al., 2004; Standish et al., 2008; Paulick et al., 2010; Mallick et al., 2014, 2015) has shown that the oceanic mantle likely consists of a heterogeneous mixture of depleted and enriched components. However, the nature of such enriched components is still debated. Mafic pyroxenite or even eclogite have been often invoked in modeling the petrogenesis of oceanic basalts, because very small amounts of such lithologies are expected to have a disproportionately large influence on the chemical and isotopic composition of the erupted lavas (e.g. Hirschmann and Stolper, 1996; Kogiso et al., 2004; Stracke and Bourdon, 2009; Waters et al., 2011; Lambart et al., 2013) due to their low-T solidi (e.g. Pertermann and Hirschmann, 2003). However, some observations do not support the direct involvement of recycled mafic pyroxenites in the generation of oceanic basalts: i) lowsolidus mantle pyroxenites start to melt at significantly higher P than peridotite (e.g. Pertermann and Hirschmann, 2003; Spandler et al., 2008), making it difficult to reconcile their presence, as a preserved lithology in the shallower melting region (1–1.5 GPa); ii) partial melts of mafic pyroxenites are highly reactive with mantle peridotite (Yaxley and Green, 1998; Mallik and Dasgupta, 2012; Sobolev et al., 2007; Wang et al., 2020; Borghini and Fumagalli, 2020), which inhibits their extraction; iii) at relatively low P, a low-solidus component would melt to rather high degrees, producing only moderately incompatible trace element-enriched partial melts (Stracke and Bourdon, 2009); and iv) pyroxenite melting residue have not been found so far in abyssal peridotites (e.g. Warren, 2016), although reactive transport modeling of mixed peridotite-pyroxenite melting indicates that pyroxenites do not melt completely (Oliveira et al., 2020).

Understanding the nature of the EMORB mantle sources is limited by the rarity of recovered pyroxenites in modern oceanic mantle settings. Numerical simulation of heterogeneous mantle partial melting has overcome this lack of natural examples by selecting some pyroxenites from ultramafic massifs as best proxies of enriched components (Lambart et al., 2009; Hirschmann et al., 2003; Brunelli et al., 2018; Oliveira et al., 2020) or by choosing modeled pyroxenite-like compositions (e.g. Kogiso et al., 1998; Standish et al., 2008; Shorttle and Maclennan, 2011). The most studied scenario is a heterogeneous mantle source composed of a very small volume (3–8%) of enriched fertile pyroxenite physically mixed into depleted peridotite (e.g. Hirschmann and Stolper, 1996; Standish et al., 2008; Waters et al., 2011; Mallick et al., 2015). The

fertile component is often thought to carry the isotopic signature of recycled material, such as subducted oceanic and/or continental crust/sediments. The Hf—Nd mantle array is interpreted as the result of mixing of melts between depleted mantle and such enriched recycled components (e.g. Stracke et al., 2003; Chauvel et al., 2008).

Alternatively, other studies have proposed that major and trace element compositions, along with the isotopic signature, of some E-MORBs do not require a "pyroxenite" component but instead represent peridotites metasomatized by the interaction with low degree melts forming an enriched - Depleted MORB Mantle (E-DMM) (Donnelly et al., 2004; Shimizu et al., 2016).

The results of our study, combined with previous work (Borghini et al., 2013, 2016, 2020) on the EL veined mantle, provide an additional scenario for the nature of the enriched component in the mantle source of E-MORBs. We found that deep melt injection and reactive crystallization of high-MgO pyroxenites produce enriched Nd—Hf isotopic mantle domains. Notably, in addition to the low &Nd-&Hf pyroxenite layers, the host peridotite also acquired enriched Nd—Hf isotopic compositions though interaction with infiltrated pyroxenite-derived melts (Fig. 4b), and this interaction modified large volumes of host peridotites. This volume of modified peridotite is much larger than that of the pyroxenite itself (Borghini et al., 2020). This in turn generated a veined mantle composed of unmodified moderately depleted MORB-type peridotite mixed with E-MORB-like domains formed by the association of rather refractory pyroxenite and metasomatized peridotite (Fig. 1b, hereafter called "EL veined mantle").

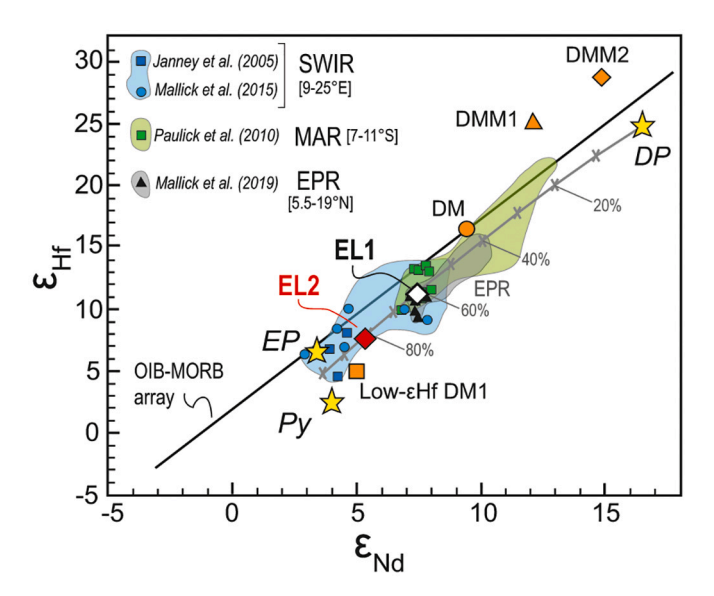


Fig. 8. Nd—Hf isotopic compositions of melts (EL1 and EL2) produced by partial melting of two modeled veined mantle sources consisting of three components: depleted peridotite (DP), enriched peridotite (EP), pyroxenite (Py). εNd-εHf values of the three components are computed at 160 Ma (explained in the text and in the Appendix A). Initial source concentrations, mineral modes and melting parameters are reported in Supplementary Table 1. We assumed as depleted peridotite DP the country peridotite ERS2/2 showing the most depleted Nd-Hf isotopic composition, the enriched peridotite EP is wall-rock peridotite GV8W and the selected pyroxenite is websterite GV10 (Table 1). The grey line shows the mixed melts produced by variable contributions of the depleted (DP) and enriched (Py + EP) end-members (numbers refer to the percentage of melt from the Py + EP component). The  $\epsilon Nd$  -  $\epsilon Hf$ values of DM, DMM and low-εHf DM1, and the MORB-OIB array, are as in Fig. 4. For comparison, we show data for EMORBs from the South-West Indian Ridge (SWIR, Janney et al., 2005; Mallick et al., 2015), Mid-Atlantic Ridge (MAR, Paulick et al., 2010) and East Pacific Rise (EPR, Mallick et al., 2019), represented by colored fields, each containing identically colored data points. These points represent several of the most enriched samples (i.e. those the lowest  $\varepsilon$ Nd and  $\varepsilon$ Hf) in each field.

In order to test the feasibility of the EL veined mantle as the potential source of low  $\varepsilon$ Nd- $\varepsilon$ Hf basalts, we modeled the decompression partial melting of multicomponent mantle sources generated by an isotopically depleted peridotite (the country peridotite) and a pyroxenite-bearing enriched peridotite. The latter consists of two components, i.e. secondary-type pyroxenite (GV10) and the associated wall-rock metasomatized peridotite. Our melting model thus assumes three components: a depleted peridotite (DP), an enriched peridotite (EP), and a high-MgO secondary-type pyroxenite (Py). In the modeling, we used the 160 Ma  $\varepsilon$ Nd and  $\varepsilon$ Hf values that represent the compositions of the EL mantle sequences at the time of exhumation (Fig. 8, details of the isotopic compositions selected for the model are in figure caption). Notably, the model using the 430 Ma  $\varepsilon$ Nd and  $\varepsilon$ Hf values (i.e. the age of pyroxenite emplacement at mantle depths, Borghini et al., 2013) provided similar results (Supplementary Fig. 1).

Our model includes two steps (details of the model are provided in Appendix A). We first estimate the melt fractions produced by the different components using the model proposed by Lambart et al. (2016), assuming a mantle source EL1 made up of 10% pyroxenite (PY), 40% enriched peridotite (EP) and 50% depleted peridotite (DP), and a more metasomatized mantle source EL2, formed by 20% pyroxenite, 50% EP and 30% DP. These calculations show that Py, EP and DP contribute to the final aggregated melt by 32%, 30% and 38%, respectively, for the EL1 source, and 50%, 32% and 18% when applied to EL2 veined mantle. Then, we calculate the Nd and Hf elemental abundances in melts produced by each component using the dynamic melting model proposed by Salters et al. (2011).

The results of our model, expressed as  $\epsilon Nd - \epsilon Hf$  values of melt derived by partial melting of EL1 and EL2 veined mantle sources, are reported in Fig. 8. In this figure, we also show the resulting mixing line, assuming that melts from the depleted (DP) and enriched (Py + EP) end-members variably mix en route to the surface to produce the erupted lavas (i.e. regardless of the solid fractions of the components in the source). Although this is a rough quantitative approach, it demonstrates that the mixing lines cover almost the entire range of Nd—Hf isotopic variation of global MORBs (Fig. 8). Melts computed assuming EL1 and EL2 sources plot along the Nd—Hf mantle array, below the DM mantle composition. EL1 aggregated melt has  $\epsilon Nd$  of +7.3 and  $\epsilon Hf$  of +11.1. Due to the higher proportion of enriched peridotite and pyroxenite over the DP component, the mantle source EL2 generates an aggregated melt with even lower  $\epsilon Nd$  (5.45) and  $\epsilon Hf$  (7.47), which plots very close to the enriched (Py + EP) components (Fig. 8).

In Fig. 8, we compare the modeling results with a compilation of MORB data from specific oceanic ridge segments where EMORB have been sampled and investigated. Overall, the computed EL melts have low  $\epsilon$ Nd- $\epsilon$ Hf signatures that match those of EMORB from the South-West Indian Ridge (SWIR, Janney et al., 2005; Mallick et al., 2015), the Mid-Atlantic Ridge (MAR, Paulick et al., 2010) and the East Pacific Rise (EPR, Mallick et al., 2019). Specifically, EL1 plots in the lower end of MAR and EPR fields overlapping with the most  $\epsilon$ Nd- $\epsilon$ Hf enriched basalts from those ridge segments. EL2 matches the compositions of SWIR basalts with the lowest  $\epsilon$ Nd- $\epsilon$ Hf values, inferred to reflect the composition of the enriched mantle components (Mallick et al., 2015) (Fig. 8).

Basalts having  $\varepsilon$ Nd and  $\varepsilon$ Hf values significantly lower than those of the DM are generally assumed to reflect the presence of an enriched component in the mantle source (e.g. Hofmann, 2014, Treatise on Geochemistry). Based on trace element and isotopic evidence, several authors have argued that the mantle sources of EMORB are lithologically heterogeneous and consist of physical mixing of depleted and enriched mantle domains (e.g. Chauvel et al., 2008; Paulick et al., 2010; Mallick et al., 2015). This view has been corroborated by several geochemical models that have evaluated the role of mantle source heterogeneity (e.g. Standish et al., 2008; Shimizu et al., 2016) as well as of melt mixing and extraction processes (e.g. Stracke and Bourdon, 2009; Rudge et al., 2013) in causing the isotopic variability of MORB.

Mallick et al. (2015) modeled the low εNd-εHf isotopic compositions

of some SWIR lavas as variable mixtures of melts derived from a veined mantle, with a small proportion ( $\approx$  5%) of a very fertile mafic pyroxenite embedded in a depleted DMM-like mantle, and variable mixing of melts derived from each component. On the same line of evidence, the trace element and isotopic variability of MORB sampled along the northern sector of EPR ocean ridge has been recently explained by variable contribution of three mantle components: depleted peridotite, enriched peridotite, and a recycled mafic component (Mallick et al., 2019). Unlike these models that necessarily require making some assumptions about the source characteristics to reproduce the basalt composition, the intriguing aspect of our numerical simulation is that it is based on direct observations (field occurrences and detailed chemical-isotopic investigations) of the potential basalts source, including the initial compositions of the mantle components and their spatial/volumetric relationships. An interesting aspect of our model is that the EL country peridotite that we assumed as the depleted mantle component (DP) also plots slightly below the mantle array. Indeed, the involvement of an ancient and strongly depleted component as the depleted end member, such as the ReLish (Salters et al., 2011), would instead shift the εNd-εHf isotopic compositions of computed melts above the mantle array away from the EMORB field.

Our model indicates that partial melting of a MORB-like veined mantle modified by pyroxenite emplacement potentially produces EMORB-like melts in terms of Nd—Hf isotopic compositions. This study provides a potential mechanism for formation of a heterogeneous mantle source, chemically and isotopically modified by deep melt infiltration and melt-peridotite interaction. In addition, it shows how such veined mantle behaves during decompression melting, which can produce Nd—Hf isotopically enriched melts, such as EMORB. Perhaps most important, our results demonstrate that, beyond their contribution during mantle melting, the presence of pyroxenitic components in the mantle plays a key role in modifying the host peridotites by interaction with pyroxenite-derived melts and creating heterogeneous mantle domains.

### 6. Concluding remarks

Spatially controlled Hf isotopic analyses across the External Liguride veined mantle reveal that pyroxenites and peridotite define a broad range of present-day  $^{176} {\rm Lu}/^{177} {\rm Hf}$  and  $^{176} {\rm Hf}/^{177} {\rm Hf}$  ratios. Their Hf and Nd isotopic variations are largely correlated and cover almost the entire MORB-OIB  $\epsilon {\rm Hf} \cdot \epsilon {\rm Nd}$  array. Pyroxenite-free country peridotites show steep trends in plots of present-day Lu/Hf vs Hf isotopes, and Sm/Nd vs Nd isotopes. In agreement with Sr—Nd isotopic signatures and combined with the DM-like fertile chemical compositions, these step trends point to a very old (Proterozoic) age of accretion to the subcontinental lithosphere of this mantle sector.

Pyroxenites show a  $\rm Lu_N/Hf_N$  variability that reflects the varying garnet abundance in the primary modal assemblage, which, with radioactive decay over time, resulted in Hf—Nd isotopic compositions covering a large portion of the OIB-MORB mantle array. The pyroxenites thus define a large range of  $\epsilon Hf$ -values, suggesting that in a single mantle sector they can represent both depleted and enriched isotopic components. The small range of initial Hf—Nd isotopic compositions at 430 Ma, that is, the age of their emplacement, suggests that the initial Hf—Nd isotopic composition of pyroxenites reflected the isotopic signature of the infiltrating melts.

Peridotites adjacent to pyroxenite layers (wall-rock and host) interacted with pyroxenite-derived melt during pyroxenite emplacement at 430 Ma. This melt-peridotite interaction resulted in the decrease in Lu/Hf ratios and the evolution to low  $\epsilon$ Hf values since then in the melt-infiltrated peridotites. Over time, such chemical and isotopic changes produced the large spread of Hf—Nd isotopic signatures observed in the External Liguride peridotites (i.e.,  $\epsilon$ Nd- $\epsilon$ Hf values at 160 Ma, which is the age of oceanic emplacement). Therefore, pyroxenite emplacement induced local metasomatism of the host peridotites that formed Hf—Nd

enriched mantle domains, making the EL veined mantle the first reported natural example of an enriched MORB-like mantle formed through the combined effect of deep emplacement of pyroxenite and pyroxenite-peridotite interaction. Decompression melting of the EL-type veined mantle is expected to produce Nd—Hf isotopically enriched melts, similar to the EMORB erupted at mid-ocean ridge settings. Our results underscore the role played by pyroxenite-derived melts in creating heterogeneous mantle domains and offer new constraints to model the origin of enriched isotope components in oceanic mantle realms.

Supplementary data to this article can be found online at https://doi.org/10.1016/j.chemgeo.2021.120591.

### **Declaration of Competing Interest**

The authors declare that they have no known competing financial interests or personal relationships that could have appeared to influence the work reported in this paper.

### Acknowledgments

Reviews by V.J.M. Salters and R. Tilhac are gratefully acknowledged. We also thank C. Chauvel for the editorial handling. This work was financially supported by the Italian Ministry of Education, University and Research (MIUR) [PRIN-2015C5LN35] "Melt rock reaction and melt migration in the MORB mantle through combined natural and experimental studies". This study was partially supported by NSF grants EAR-GeoPRISIMS 1457293 and EAR-1714892 to YC.

### Appendix A

Melt productivity of the EL veined mantle source. Melt fractions produced by the different components were derived using the model proposed by Lambart et al. (2016), which simulates the isentropic decompression melting of pyroxenite-peridotite mantle sources, by taking into account the bulk composition and solid fraction of pyroxenite in the source. The model assumes the parameterization of Katz et al. (2003) for the melting functions of a fertile peridotite that is in good agreement with the rather fertile bulk composition of the EL peridotites (both country and pyroxenite-bearing) selected for this study. Based on field observations and chemical profiles on the EL mantle sequences (Borghini et al., 2020), we assumed a mantle source EL1 made up of 10% pyroxenite (PY), 40% enriched peridotite (EP) and 50% depleted peridotite (DP). We also investigated a more metasomatized mantle source EL2, formed by 20% pyroxenite, 50% EP and 30% DP. Assuming a potential temperature (T<sub>P</sub>) of 1350 °C and complete extraction of aggregated melts at 1 GPa, peridotites and pyroxenite experience the following melting degrees: 8% and 34% respectively for the EL1 mantle source; 7% and 29% for the EL2 assemblage. Peridotite partial melting occurs within the spinel stability field at P < 2 GPa. If we assume that the partial melts from each lithology are perfectly mixed during melt extraction at 1 GPa, then the contribution in terms of liquid mass fraction of each component (LF<sub>C</sub>) to the final aggregated melt can be derived by the equation LF\_{C1} = ( $\Psi_{C1} \times F_{C1}$ )/[( $\Psi_{C1} \times F_{C1}$ ) + ( $\Psi_{C2} \times F_{C2}$ ) + ( $\Psi_{C3}$  $\times$  F<sub>C3</sub>)], where  $\Psi$  and F<sub>C</sub> are mass fraction and melt fraction of the component C in the source, respectively.

Calculations of the composition of aggregated melts. The Nd and Hf elemental abundances in melts produced by each component were calculated using the dynamic melting model proposed by Salters et al. (2011). We assume a residual porosity of 0.1%, an amount of melt extracted at each step of 0.2% and 0.3% of melting per Km. The initial source concentrations, mineral modes and melting parameters are reported in Supplementary Table 1. For partial melting of peridotites EP and DP in the spinel stability field, we used the melting modes and the partition coefficients determined by Salters and Longhi (1999), Longhi (2002) and Salters et al. (2002). Partial melting of pyroxenite GV10 (Py)

is 5% in the garnet stability field and proceeds up to 29–32% in the spinel stability field; for the Py component, we used the melting reactions experimentally derived by Borghini et al. (2017) (Supplementary Table 1). The final composition of aggregated melts has been computed by mixing the melt composition of each component using the melt proportions estimated by the first step of the model (see above).

#### References

- Ackerman, L., Bizimis, M., Haluzová, E., Sláma, J., Svojtka, M., Hirajima, T., Erban, V., 2016. Re–Os and Lu–Hf isotopic constraints on the formation and age of mantle pyroxenites from the Bohemian Massif. Lithos 256–257, 197–210.
- Allègre, C.J., Turcotte, D.L., 1986. Implications of a two-component marble-cake mantle. Nature 323, 123–127.
- Anders, E., Grevesse, N., 1989. Abundances of the elements: meteoric and solar. Geochim. Cosmochim. Acta 53, 197–214.
- Bizimis, M., Sen, G., Salters, V.J., Keshav, S., 2005. Hf-Nd-Sr isotope systematics of garnet pyroxenites from Salt Lake Crater, Oahu, Hawaii: evidence for a depleted component in Hawaiian volcanism. Geochim. Cosmochim. Acta 69, 2629–2646.
- Blichert-Toft, J., Albarede, F., Kornprobst, J., 1999. Lu-Hf isotope systematics of garnet pyroxenites from Beni Bousera, Morocco: implications for basalt origin. Science 283, 1303–1306 (1999).
- Bodinier, J.-L., Vasseur, G., Vernieres, J., Dupuy, C., Fabries, J., 1990. Mechanisms of mantle metasomatism: geochemical evidence from the Lherz orogenic peridotite. J. Petrol. 31, 597–628.
- Bodinier, J.L., Menzies, M.A., Thirlwall, M.F., 1991. Continental to oceanic mantle transition: REE and Sr–Nd isotopic geochemistry of the Lanzo Lherzolite Massif. J. Petrol. 191–210 (Special Lherzolite Issue).
- Bodinier, J.L., Menzies, M.A., Shimizu, N., Frey, F.A., McPherson, E., 2004. Silicate, hydrous and carbonate metasomatism at Lherz, France: contemporaneous derivatives of silicate melt-harzburgite reaction. J. Petrol. 45, 299–320.
- Borghini, G., Rampone, E., Zanetti, A., Class, C., Cipriani, A., Hofmann, A.W., Goldstein, S., 2013. Meter-scale Nd isotopic heterogeneity in pyroxenite-bearing Ligurian peridotites encompasses global-scale upper mantle variability. Geology 41, 1055–1058.
- Borghini, G., Rampone, E., Zanetti, A., Class, C., Cipriani, A., Hofmann, A.W., Goldstein, S., 2016. Pyroxenite layersin the Northern Apennines upper mantle (Italy) generation by pyroxenite melting and melt infiltration. J. Petrol. 57, 625–653.
- Borghini, G., Fumagalli, P., 2020. Melting relations of anhydrous olivine-free pyroxenite Px1 at 2 GPa. Eur. J. Mineral. 32, 251–264.
- Borghini, G., Fumagalli, P., Rampone, E., 2017. Partial melting experiments on a natural pyroxenite at 1 and 1.5 GPa: insights on the role of secondary pyroxenites in basalts generation. Contrib. Mineral. Petrol. 172, 70.
- Borghini, G., Rampone, E., Zanetti, A., Class, C., Fumagalli, P., Godard, M., 2020. Ligurian pyroxenite-peridotite sequences (Italy) and the role of melt-rock reaction in creating enriched-MORB mantle source. Chem. Geol. 532, 119252.
- Bouvier, A., Vervoort, J.D., Patchett, P.J., 2008. The Lu–Hf and Sm–Nd isotopic composition of CHUR: constraints from unequilibrated chondrites and implications for the bulk composition of terrestrial planets. Earth Planet. Sci. Lett. 273, 48–57.
- Brown, E.L., Lesher, C.E., 2014. North Atlantic magmatism controlled by temperature, mantle composition and buoyancy. Nat. Geosci. 7, 820–824.
- Brown, E.L., Lesher, C.E., 2016. REEBOX PRO: a forward model simulating melting of thermally and lithologically variable upwelling mantle. Geochem. Geophys. Geosyst. 17, 3929–3968.
- Brunelli, D., Cipriani, A., Bonatti, E., 2018. Thermal effects of pyroxenites on mantle melting below mid-ocean ridges. Nat. Geosci. 11, 520–525.
- Byerly, B.L., Lassiter, J.C., 2014. Isotopically ultradepleted domains in the convecting upper mantle: implications for MORB petrogenesis. Geology 42, 203–206.
- Cai, Y., LaGatta, A., Goldstein, S.L., Langmuir, C.H., Gomez-Tuena, A., Martin-del Pozzo, G., Carrasco-Nunez, G., 2014. Hafnium isotope evidence for slab melt contributions in the Central Mexican Volcanic Belt and implications for slab melting in hot and cold slab arcs. Chem. Geol. 377, 45–55.
- Chauvel, C., Lewin, E., Carpentier, M., Arndt, N.T., Marini, J.-C., 2008. Role of recycled oceanic basalt and sediment in generating the Hf–Nd mantle array. Nat. Geosci. 1, 64–67.
- Donnelly, K.E., Goldstein, S.L., Langmuir, C.H., Spiegelman, M., 2004. Origin of enriched ocean ridge basalts and implications for mantle dynamics. Earth Planet. Sci. Lett. 226, 347–366.
- Elkins, L.J., Bourdon, B., Lambart, S., 2019. Testing pyroxenite versus peridotite sources for marine using U-series isotopes. Lithos 332–333, 226–244.
- Faure, G., 1986. Principles of Isotope Geology. John Wiley and Sons, New York. Griffin, W.L., Pearson, N.J., Belousoya, E., Jackson, S.E., van Achterbergh, E., O'Reilly
- Griffin, W.L., Pearson, N.J., Belousova, E., Jackson, S.E., van Achterbergh, E., O'Reilly, S. Y., Shee, S.R., 2000. The Hf isotope composition of cratonic mantle: LAM-MC-ICPMS analysis of zircon megacrysts in kimberlites. Geochim. Cosmochim. Acta 64, 133–147.
- Herzberg, C., 2011. Identification of source lithology in the Hawaiian and Canary Islands: implications for origins. J. Petrol. 52, 113–146.
- Hezberg, C., Vidito, C., Starkey, N.A., 2016. Nickel-Cobalt contents of olivine record origins of mantle peridotite and related rocks. Am. Mineral. 101, 1952–1966.
- Hidas, K., Borghini, G., Tommasi, A., Zanetti, A., Rampone, E., 2021. Interplay between melt infiltration and deformation in the deep lithospheric mantle (External Liguride ophiolitie, North Italy). Lithos 380–381, 105855.

Hirschmann, M.M., Stolper, E.M., 1996. A possible role for garnet pyroxenite in the origin of the 'garnet signature' in MORB. Contrib. Mineral. Petrol. 124, 185–208.

- Hirschmann, M.M., Kogiso, T., Baker, M.B., Stolper, E.M., 2003. Alkalic magmas generated by partial melting of garnet pyroxenite. Geology 31, 481–484.
- Hofmann, A.W., 2014. Sampling mantle heterogeneity through oceanic basalts: isotopes and trace elements. In: Carlson, R.W., Holland, H.D., Turekian, K.K. (Eds.), Treatise on Geochemistry, the Mantle and Core. Elsevier, Oxford, pp. 61–101.
- Jacobsen, S., Wasserburg, G.J., 1980. Sm-Nd isotopic systematics of Chondrites and Achondrites. Meteoritics 15, 307.
- Janney, P.E., Le Roex, A.P., Carlson, R.W., 2005. Hafnium isotope and trace element constraints on the nature of mantle heterogeneity beneath the central South-west Indian Ridge (13 degrees E to 47 degrees E). J. Petrol. 46, 2427–2464.
- Jweda, J., Bolge, L., Class, C., Goldstein, S.L., 2016. High precision Sr-Nd-Hf-Pb isotopic compositions of USGS reference material BCR-2. Geostand. Geoanal. Res. 40, 101–115
- Katz, R.F., Spiegelman, M., Langmuir, C.H., 2003. A new parameterization of hydrous mantle melting. Geochem. Geophys. Geosyst. 4 (1073), GC000433.
- Kogiso, T., Hirose, K., Takahashi, E., 1998. Melting experiments on homogeneous mixtures of peridotite and basalt: application to the genesis of ocean island basalts. Earth Planet. Sci. Lett. 162, 45–61.
- Kogiso, T., Hirschmann, M.M., Pertermann, M., 2004. High-pressure partial melting of mafic lithologies in the mantle. J. Petrol. 45, 2407–2422.
- Lambart, S., 2017. No direct contribution of recycled crust in Icelandic basalts. Geochem. Perspect. Lett. 4, 7–12.
- Lambart, S., Laporte, D., Schiano, P., 2009. An experimental study of pyroxenite partial melts at 1 and 1·5 GPa: implications for the major-element composition of mid-ocean ridge basalts, Earth Planet. Sci. Lett. 288, 335–347.
- Lambart, S., Laporte, D., Provost, A., Schiano, P., 2012. Fate of pyroxenite-derived melts in the peridotitic mantle: thermodynamic and experimental constraints. J. Petrol. 53, 451–476.
- Lambart, S., Baker, M.B., Stolper, E.M., 2016. The role of pyroxenite in basalt genesis: Melt-PX, a melting parameterization for mantle pyroxenites between 0.9 and 5 GPa. J. Geophys. Res. 121, 5708–5735.
- Lambart, S., Laporte, D., Schiano, P., 2013. Markers of the pyroxenite contribution in the major-element compositions of oceanic basalts: review of the experimental constraints. Lithos 160-161, 14–36.
- Longhi, J., 2002. Some phase equilibria systematics of lherzolite melting: I. Geochem. Geophys. Geosyst. 3, GC000204.
- Lu, J., Griffin, W.L., Tilhac, R., Xiong, Q., Zheng, J., O'Reilly, S.Y., 2018. Tracking deep litho- spheric events with Garnet-Websterite Xenoliths from Southeastern Australia. J. Petrol. 59, 901–930.
- Mallick, S., Sachi-Kocher, A., Dick, H.J.B., Salters, V., 2014. Isotope and trace element insights into heterogeneity of sub-ridge mantle. Geochem. Geophys. Geosyst. 15, 2438–2453.
- Mallick, S., Standish, J.J., Bizimis, M., 2015. Constraints on the mantle mineralogy of an ultra-slow ridge: Hafnium isotopes in abyssal peridotites and basalts from the 9-25°E Southwest Indian Ridge. Earth Planet. Sci. Lett. 410, 42–53.
- Mallick, S., Salters, V.J.M., Langmuir, C.H., 2019. Geichemical variability along the Northern East Pacific Rise: coincident source composition and ridge segmentation. Geochem. Geophys. Geosyst. 20, 1889–1911.
- Mallik, A., Dasgupta, R., 2012. Reaction between MORB-eclogite derived melts and fertile peridotite and generation of ocean island basalts. Earth Planet. Sci. Lett. 329–330, 97–108
- Mallik, A., Dasgupta, R., 2013. Reactive infiltration of MORB-eclogite-derived carbonated silicate melt into fertile peridotite at 3 GPa and genesis of alkali magmas. J. Petrol. 54, 2267–2300.
- Marroni, M., Molli, G., Montanini, A., Tribuzio, R., 1998. The association of continental crust rocks with ophiolites in the Northern Apennines (Italy): implications for the continent-ocean transition in the Western Tethys. Tectonophysics 292, 43–66.
- Marroni, M., Meneghini, F., Pandolfi, L., 2010. Anatomy of the Lçigure-Piemontese subduction system: evidence from Late Cretaceous-middle Eocene convergent margin deposits in the Northern Apennines, Italy. Int. Geol. Rev. 52, 1160–1192.
- Montanini, A., Tribuzio, R., 2015. Evolution of recycled crust within the mantle: constraints from the garnet pyroxenites of the External Ligurian ophiolites (northern Apennines, Italy). Geology 43, 911–914.
- Montanini, A., Tribuzio, R., Anczkiewicz, R., 2006. Exhumation history of a garnet pyroxenite-bearing mantle section from a continent-ocean transition (Northern Apennine ophiolites, Italy). J. Petrol. 47, 1943–1971.
- Montanini, A., Tribuzio, R., Thirlwall, M., 2012. Garnet clinopyroxenite layers from the mantle sequences of the Northern Apennine ophiolites (Italy): evidence for recycling of crustal material. Earth Planet. Sci. Lett. 351–352, 171–181.
- Mukasa, S.B., Shervais, J.W., 1999. Growth of sub-continental lithosphere: evidence from repeated injections in the Balmuccia lherzolite massif, Italian Alps. Lithos 48, 287–316.
- Oliveira, B., Afonso, J.C., Tilhac, R., 2020. A disequilibrium reactive transport model for mantle magmatism. J. Petrol. 61, egaa067.
- Paulick, H., Mueker, C., Schluth, S., 2010. The influence of small-scale mantle heterogeneities on Mid-Ocean Ridge volcanism: evidence from the southern Mid-Atlantic Ridge (7 degrees 30'S to 11 degrees 30'S) and Ascension Island. Earth Planet. Sci. Lett. 296, 299–310.
- Pearson, D.G., Nowell, G.M., 2004. Re-Os and Lu-Hf isotope constraints on the origin and age of pyroxenites from the Beni Bousera peridotite massif: implications for mixed peridotite-pyroxenite mantle source. J. Petrol. 45, 439–455.
- Pearson, D.G., Davies, G.R., Nixon, P.H., 1993. Geochemical constraints on the petrogenesis of diamond facies pyroxenites from the Beni Bousera peridotite massif, North Morocco. J. Petrol. 34, 125–172.

G. Borghini et al.

- Pertermann, M., Hirschmann, M.M., 2003. Partial melting on a MORB-like pyroxenite between 2 and 3 GPa: constraints on the presence of pyroxenite in basalt source regions from solidus location and melting rate. J. Geophys. Res. 108, 2125.
- Rampone, E., Hofmann, A.W., 2012. A global overview of isotopic heterogeneities in the oceanic mantle. Lithos 148, 247–261.
- Rampone, E., Piccardo, G.B., 2000. The ophiolite-oceanic lithosphere analogue: new insights from the Northern Apennine (Italy). In: Dilek, J., Moores, E., Elthon, D., Nicolas, A. (Eds.), Ophiolites and Oceanic Crust: New Insights From Field Studiesand Ocean Drilling Program, vol. 349. Geological Society of America, Special Paper, pp. 21–34.
- Rampone, E., Sanfilippo, A., 2021. The heterogeneous Tethyan oceanic lithosphere of the Alpine ophiolites. Elements: Int. Mag. Mineral. Geochem. Petrol. 17 (1), 23–28.
- Rampone, E., Hofmann, A.W., Piccardo, G.B., Vannucci, R., Bottazzi, P., Ottolini, L., 1995. Petrology, mineral and isotope geochemistry of the External Liguride peridotites (Northern Apennines, Italy). J. Petrol. 123, 61–76.
- Rampone, E., Borghini, G., Basch, V., 2020. Melt migration and melt-rock reaction in the Alpine-Apennine peridotites: insights on mantle dynamics in extending lithosphere. Geosci. Front. Spec. Issue 11, 151–166.
- Rudge, J.F., Maclennan, J., Stracke, A., 2013. E geochemical consequences of mixing melts from a heterogeneous mantle. Geochim. Cosmochim. Acta 114, 112–143.
- Salters, V.J.M., Longhi, J.E., 1999. Trace element partitioning during the initial stages of melting beneath ocean ridges. Earth Planet. Sci. Lett. 166, 15–30.
- Salters, V.J.M., Stracke, A., 2004. Composition of the depleted mantle. Geochem. Geophys. Geosyst. 5, Q05B07.
- Salters, V.J.M., Longhi, J.E., Bizimis, M., 2002. Near mantle solidus trace element partitrioning at pressures up to 3.4 GPa. Geochem. Geophys. Geosyst. 3 (6) https:// doi.org/10.1029/2001GC000148.
- Salters, V.J.M., Mallick, S., Hart, S.R., Langmuir, C.H., Stracke, A., 2011. Domains of depleted mantle; new evidence from hafnium and neodymium isotopes. Geochem. Geophys. Geosyst. 12, Q08001.
- Sanfilippo, A., Salters, V., Tribuzio, R., Zanetti, A., 2019. Role of ancient, ultra-depleted mantle in Mid-Ocean-Ridge magmatism. Earth Planet. Sci. Lett. 511, 89–98.
- Shimizu, K., Saal, A.E., Myers, C.E., Nagle, A.N., Hauri, E.H., Forsyth, D.W., Kamenetsky, V.S., Niu, Y., 2016. Two-component mantle melting-mixing model for the generation of mid-ocean ridge basalts: implications for the volatile content of the Pacific upper mantle. Geochim. Cosmochim. Acta 176, 44–80.
- Shorttle, O., Maclennan, J., 2011. Compositional trends of Icelandic basalts: implications for short-length scale lithological heterogeneity in mantle plumes. Geochem. Geophys. Geosyst. 12, Q11008.
- Snow, J.E., Schmidt, G., Rampone, E., 2000. Os isotopes and highly siderophile elements (HSE) in the Ligurian ophiolites, Italy. Earth Planet. Sci. Lett. 175, 119–132.
- Sobolev, A.V., Hofmann, A.W., Sobolev, S.V., Nikogosian, I.K., 2005. An olivine-free mantle source of Hawaiian shield basalts. Nature 434, 590–597.
- Sobolev, A.V., Hofmann, A.W., Kuzmin, D.V., Yaxley, G.M., Arndt, N.T., Chung, S.L., Danyushevsky, L.V., Elliott, T., Frey, F.A., Garcia, M.O., Gurenko, A.A., Kamenetsky, V.S., Kerr, A.C., Krivolutskaya, N.A., Matvienkov, V.V., Nikogosian, I. K., Rocholl, A., Sigurdsson, I.A., Sushchevskaya, N.M., Teklay, M., 2007. The amount of recycled crust in sources of mantle-derived melts. Science 316. 412–417.
- Spandler, C., Yaxley, G.M., Green, D.H., Rosenthal, A., 2008. Phase relations and melting of anhydrous K-bearing eclogite from 1200 to 1600°C and 3 to 5 GPa. J. Petrol. 49, 771–795.
- Standish, J.J., Dick, H.J.B., Michael, P.J., Melson, W.G., O'Hearn, T., 2008. MORB generation beneath the ultraslow spreading Southwest Indian Ridge (9–25°E): major element chemistry and the importance of process versus source. Geochem. Geophys. Geosyst. 9, Q05004.

- Stracke, A., 2012. Earth's heterogeneous mantle: a product of convection-driven interaction between crust and mantle. Chem. Geol. 330–331, 274–299.
- Stracke, A., Bourdon, B., 2009. The importance of melt extraction for tracing mantle heterogeneity. Geochim. Cosmochim. Acta 73, 218–238.
- Stracke, A., Bizimis, M., Salters, V.J.M., 2003. Recycling of oceanic crust: quantita-tive constraints. Geochem. Geophys. Geosyst. 4, 8003.
- Stracke, A., Snow, J.E., Hellebrand, E., von der Handt, A., Bourdon, B., Birbaum, K., Gunther, D., 2011. Abyssal peridotite Hf isotopes identify extreme mantle depletion. Earth Planet. Sci. Lett. 308, 359–368.
- Sun, S.S., Hanson, G.N., 1975. Origin of Ross Island basanitoids and limitations upon the heterogeneity of mantle sources for alkali basalts and nephelinites. Contrib. Mineral. Petrol. 55. 77–106.
- Tilhac, R., Ceuleneer, G., Griffin, W.L., O'Reilly, S.Y., Pearson, N.J., Benoit, M., Henry, H., Girardeau, J., Gregoire, M., 2016. Primitive arc magmatism and delamination: petrology and geochemistry of pyroxenites from the Cabo Ortegal Complex, Spain. J. Petrol. 57, 1921–1954.
- Tilhac, R., Oliveira, B., Griffin, W.L., O'Reilly, S.Y., Schaefer, B.F., Alard, O., Ceuleneer, G., Afonso, J.C., Grégoire, M., 2020. Reworking of old continental lithosphere: unradiogenic Os and decoupled Hf-Nd isotopes in sub-arc mantle pyroxenites. Lithos 354–355, 105346.
- Vannucci, R., Piccardo, G.B., Rivalenti, G., Zanetti, A., Rampone, E., Ottolini, L., Oberti, R., Mazzucchelli, M., Bottazzi, P., 1995. Origin of LREE-depleted amphiboles in the subcontinental mantle. Geochim. Cosmochim. Acta 59, 1763–1771.
- Varas-Reus, M.I., Garrido, C.J., Marchesi, C., Bosch, D., Hidas, K., 2018. Genesis of ultrahigh pressure garnet pyroxenites in orogenic peridotites and its bearing on the compositional heterogeneity of the Earth's mantle. Geochim. Cosmochim. Acta 232, 303–328.
- Vervoort, J.D., Patchett, P.J., Blichert-Toft, J., Albarede, F., 1999. Relationships between Lu–Hf and Sm–Nd isotopic systems in the global sedimentary system. Earth Planet. Sci. Lett. 168, 79–99.
- Wang, C., Lo Cascio, M., Liang, Y., Xu, W., 2020. An experimental study of peridotite dissolution in eclogite-derived melts: implications for styles of melt-rock interaction in lithospheric mantle beneath the North China Craton. Geochim. Cosmochim. Acta 278, 157–176.
- Warren, J.M., 2016. Global variations in abyssal peridotite compositions. Lithos 248–251, 193–219.
- Warren, J.M., Shimizu, N., Sakaguchi, C., Dick, H.J.B., Nakamura, E., 2009. An assessment of upper mantle heterogeneity based on abyssal peridotite isotopic compositions. J. Geophys. Res. 114, B12203.
- Waters, C.L., Sims, K.W.W., Perfit, M.R., Blichert-Toft, J., Blusztajn, J., 2011. Perspective on the genesis of E-MORB from chemical and isotopic heterogeneity at 9–10°N East Pacific Rise. J. Petrol. 52, 565–602.
- Weis, D., Kieffer, B., Hanano, D., Silva, I.N., Berling, J., Pretorius, W., Maerschalk, C., Mattielli, N., 2007. Hf isotope compositions of U.S. Geological survey reference materials. Geochem. Geophys. Geosyst. 8, Q06006.
- Workman, R.K., Hart, S.R., 2005. Major and trace element composition of the depleted MORB mantle (DMM). Earth Planet. Sci. Lett. 231, 53–72.
- Yaxley, G.M., Green, D.H., 1998. Reactions between eclogite and peridotite: mantle refertilisation by subduction of oceanic crust. Schweiz. Mineral. Petrogr. Mitt. 78, 243–255.
- Zanetti, A., Vannucci, R., Bottazzi, P., Oberti, R., Ottolini, L., 1996. Infiltration metasomatism at Lherz as monitored by systematic ion-microprobe investigations close to a hornblendite vein. Chem. Geol. 134, 113–133.